VTT PUBLICATIONS 720

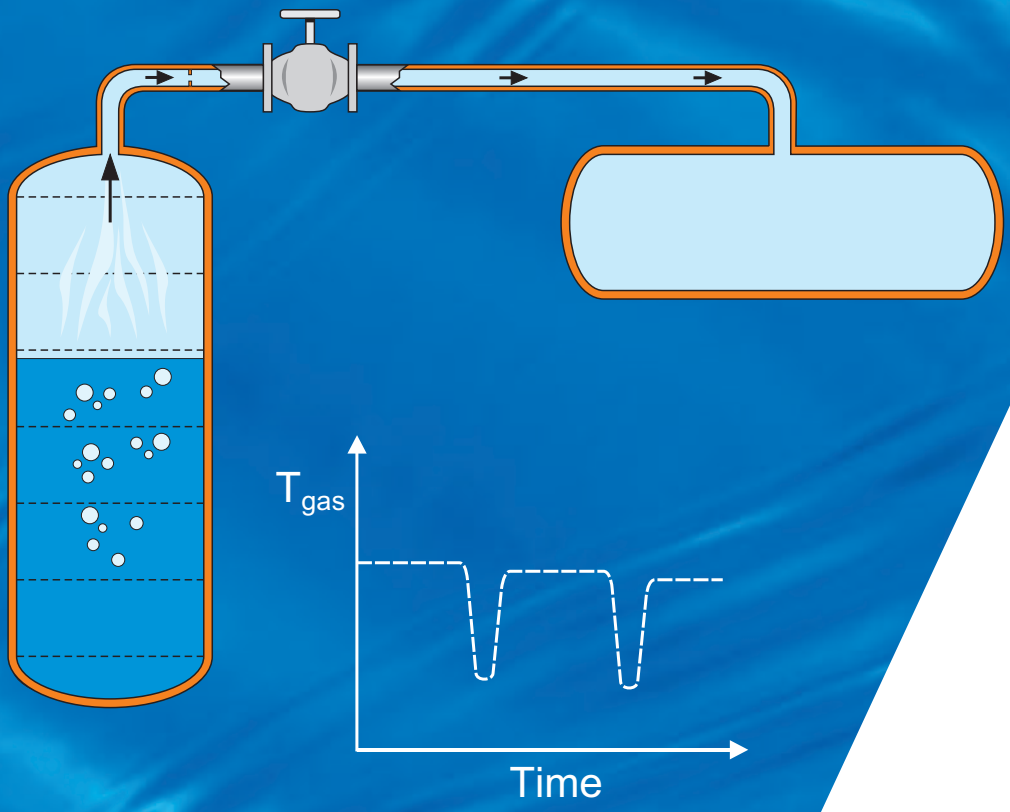

Markku Hänninen

Phenomenological extensions to APROS six-equation model

Non-condensable gas, supercritical pressure, improved CCFL and reduced numerical diffusion for scalar transport calculation

VTT PUBLICATIONS 720

Phenomenological extensions to APROS six-equation model

Non-condensable gas, supercritical pressure, improved CCFL and reduced numerical diffusion for scalar transport calculation

Markku Hänninen

VTT

Dissertation for the degree of Doctor of Technology to be presented with due permission of Department of Nuclear Energy at Lappeenranta University of Technology for public examination and debate in Auditorium 1381 on the 27th of November, 2009, at noon.

ISBN 978-951-38-7367-7 (soft back ed.)
ISSN 1235-0621 (soft back ed.)

ISBN 978-951-38-7368-4 (URL: http://www.vtt.fi/publications/index.jsp)
ISSN 1455-0849 (URL: http://www.vtt.fi/publications/index.jsp)

JULKAISIJA – UTGIVARE – PUBLISHER

VTT, Vuorimiehentie 3, PL 1000, 02044 VTT
puh. vaihde 020 722 111, faksi 020 722 4374

VTT, Bergsmansvägen 3, PB 1000, 02044 VTT
tel. växel 020 722 111, fax 020 722 4374

VTT Technical Research Centre of Finland, Vuorimiehentie 3, P.O. Box 1000, FI-02044 VTT, Finland
phone internat. +358 20 722 111, fax + 358 20 722 4374

Technical editing Maini Manninen

Edita Prima Oy, Helsinki 2009

Markku Hänninen. Phenomenological extensions to APROS six-equation model. Non-condensable gas, supercritical pressure, improved CCFL and reduced numerical diffusion for scalar transport calculation [Kuusiyhtälömallin ilmiövalikoiman laajentaminen. Lauhtumattomien kaasujen ja ylikriittisen paineen laskenta, veden ja höyryn vastakkaissuuntaisen virtauksen mallien parantaminen ja numeerisen tasoittumisen vähentäminen]. VTT Publications 720. 60 p. + app. 62 p.

Keywords Two-fluid model, two-phase flow, interface heat transfer, interface friction, wall friction, wall heat transfer, boiling crisis, non-condensable gas, dissolved gas, counter current flow limitation, discreatization, validation, supercritical pressure, nuclear power plant, APROS

Abstract

This thesis focuses on the development of the two-fluid model of the APROS simulation program. The system of constitutive equations and how equations are related to basic equations have been presented and discussed. The new non-condensable gas model, which was implemented to the two-fluid model, has been described in detail. The extension of the non-condensable gas model to the two-fluid system and the validation of the model have also been presented. The changes made to the six-equation model when the model has been applied to supercritical pressure calculation have been depicted. Finally, the author describes how the whole complicated system is verified and validated. Through the simulations, the applicability of the two-phase model for the analyses of real plant applications is substantiated and verified.

In addition to this summary, the thesis consists of four publications. The first paper deals with how the CCFL (Counter Current Flow Limitation) correlations have been implemented to the code and how these correlations have been verified. In the second paper, the non-condensable gas model and its implementation to the two-fluid model have been presented. The third paper describes how the sharp temperature distribution can be maintained in the liquid flow through the aid of simple higher order discretization. In the fourth paper, the modifications carried out to the two-fluid model when applied to the calculation of the supercritical pressure flow are described and discussed.

Markku Hänninen. Phenomenological extensions to APROS six-equation model. Non-condensable gas, supercritical pressure, improved CCFL and reduced numerical diffusion for scalar transport calculation [Kuusiyhtälömallin ilmiövalikoiman laajentaminen. Lauhtumattomien kaasujen ja ylikriittisen paineen laskenta, veden ja höyryn vastakkaissuuntaisen virtauksen mallien parantaminen ja numeerisen tasoittumisen vähentäminen]. VTT Publications 720. 60 p. + app. 62 p.

Keywords Two-fluid model, two-phase flow, interface heat transfer, interface friction, wall friction wall heat transfer, boiling crisis, non-condensable gas, dissolved gas, counter current flow limitation, discreatization, validation, supercritical pressure, nuclear power plant, APROS

Tiivistelmä

Tämä väitöskirja kuvaa APROS-simulointiohjelmistoon kuuluvan yksidimensioisen veden kaksifaasivirtauksen laskentaan tarkoitetun kuusiyhtälömallin kehityksen. Korrelaatiotyyppiset lisäyhtälöt kuvataan ja samalla kerrotaan, kuinka ne liittyvät perusyhtälöiden muodostamaan ratkaisuun. Perinteisen kaksifaasilaskentamallin lisäksi väitöskirja kuvaa lauhtumattomien kaasujen laskentamallin, sen kelpoistamisen ja kuinka tämä laskentamalli liittyy kaksifaasivirtauksen ratkaisujärjestelmään. Kaksifaasimallia on myös muutettu siten, että sitä voidaan soveltaa ylikriittisen paineen laskentaan. Kaksifaasimalli muodostaa hyvin monimutkaisen järjestelmän, jonka toimivuus pitää varmentaa aina kun jokin uusi osamalli liitetään kokonaisuuteen tai jotakin mallin osaa muutetaan. Väitöskirjassa kuvataan eräiden kaksifaasivirtaukseen ja lämmönsiirtoon liityvien kelpoistamiseen käytettyjen kokeiden laskentaa. Näillä kokeilla osoitetaan kaksifaasimallin toimivuus ja se, että laskentatulokset vastaavat todellisuutta.

Johdannon lisäksi väitöskirja sisältää liitteenä olevat neljä julkaisua. Ensimmäisessä kuvataan faasien vastakkaissuuntaisen virtauksen rajoittamiseen käytettyjen CCFL-korrelaatioiden (Counter Current Flow Limitation) liittäminen laskentajärjestelmään sekä näiden korrelaatioiden kelpoistamiseen liittyvät simuloinnit. Toisessa kerrotaan yksityiskohtaisesti lauhtumattomien kaasujen laskentamallista, sen kelpoistamisesta ja soveltamisesta todelliseen laitostransientin laskentaan. Kolmannessa julkaisussa kuvataan ohjelmaan kehitetty vaihtoehtoinen korkeamman kertaluvun diskretointimenetelmä, jolla pystytään vähentämään numeerista diffuusiota. Neljännessä julkaisussa tarkastellaan ylikriittisen paineen laskennan vaatimia muutoksia kaksifaasimalliin ja kuvataan mallin toimivuutta mittaavien laskentatapauksien simulointeja.

Academic dissertation

Supervisor Professor, Dr. Tech Riitta Kyrki-Rajamäki
LUT Energy
Faculty of Technology
Lappeenranta University of Technology
Finland

Reviewers Professor F.D'Auria
Nuclear Reactor Thermo Hydraulics
University of Pisa
Italy

Docent, Dr. Tech Juhani Hyvärinen
Executive Vice President, Nuclear Engineering
Fennovoima Ltd
Finland

Opponent Docent, Dr. Heinz G. Sonnenburg
Gesellschaft für Anlagen- und Reaktorsicherheit (GRS) mbH
Munich
Germany

Preface

This work has been carried out at VTT Technical Research Centre of Finland in connection with the development project for APROS simulation code. The development program is a common effort of VTT and Fortum Nuclear Services Ltd. The validation work of the six-equation model has been made largely in national SAFIR and SAFIR2010 -research programs funded by State Nuclear Waste Management Fund (VYR), VTT and other funders.

I thank my supervisor, Prof. Riitta Kyrki-Rajamäki, for her constant interest and encouragement in preparation of this thesis.

I am grateful to reviewers of the thesis, Dr. Francesco D'Auria and Dr. Juhani Hyvärinen, who have provided valuable recommendations in improving the thesis.

In particular I wish to thank coauthors of my publications Mr. Joona Kurki, Mr. Esa Ahtinen, Dr. Jari Tuunanen and LicTech Juhani Vihavainen.

The code development and its validation is teamwork, and therefore I am grateful to many of my colleagues at VTT and Fortum Nuclear Services. Especially I wish to thank Mr. Jukka Ylijoki, who is indispensable in keeping the six-equation model and other models in APROS workable.

Finally, I would like to thank my wife, Marja-Leena for her patience during this effort.

Espoo, November 2009 Markku Hänninen

List of publications

This thesis includes the summary provided and the following four publications:

I Hänninen, M. Implementation and validation of downcomer and upper tie plate CCFL correlations in a two-fluid code. Proceedings of the 16th International Conference on Nuclear Engineering, ICONE16, May 11–15, 2008, Orlando, Florida, USA.

II Hänninen, M. & Ahtinen, E. Simulation of non-condensable gas flow in two-fluid model of APROS – Description of the model, validation and application. Annals of Nuclear Energy 36 (2009), pp. 1588–1596.

III Vihavainen, J., Hänninen, M. & Tuunanen, J. Improved thermal stratification modeling in the APROS code simulations of passive safety injection experiments. Ninth International Topical Meeting in Nuclear Reactor Thermal Hydraulics (NURETH-9), San Francisco, California, October 3–8, 1999.

IV Hänninen, M. & Kurki, J. Simulation of flows at supercritical pressures with a two-fluid code. NUTHOS-7: The 7th International Topical Meeting on Nuclear Reactor Thermal Hydraulics, Operation and Safety, Seoul, Korea, October 5–9, 2008.

Author's contribution

In Publication I, the author describes how the CCFL (Counter Current Flow Limitation) -correlations have been implemented to the six-equation model of APROS code. In addition, how these correlations have been verified is described.

In Publication II the the non-condensable gas model made and implemented by the author has been presented. In addition, the co-author describes the simulated application in a real nuclear power plant.

In Publication III, the author has developed and implemented the higher order discretization model. It has been shown that by the aid of this model the sharp temperature distributions can be better maintained in the liquid flow. The co-authors have validated the model.

In Publication IV, the author modified the two-fluid model in such a way that it can be applied to the calculation of the supercritical pressure flow. The co-author has taken part in improving and testing the model developed.

Contents

Appendices III and IV of this publication are not included in the PDF version. Please order the printed version to get the complete publication (http://www.vtt.fi/publications/index.jsp).

Nomenclature

A	area, flow area (m^2)
Bo	Bond number
f	friction factor
E	rate of entrainment
F	friction (N/m^3)
g	acceleration of gravitation (m/s^2)
h	enthalpy (J/kg)
j	superficial velocity (m/s)
K	interface heat transfer coefficient, Kutatelaze number
M	mole weight
$\dot{m}$	mass flow (kg/s)
p	pressure (Pa)
q	heat flow/volume
R	universal gas constant (8.314kJ/kmol K)
T	temperature (ºC or K)
t	time (s)
u	velocity (m/s)
V	volume (m^3)
z	space coordinate in flow direction (m)
x	mass fraction
α	gas volume fraction
γ	ratio of specific heats (ideal gas)
ρ	density (kg/m^3)
Γ	mass transfer ($kg/s\ m^3$)
Δt	time step (s)
τ	time constant (s)
σ	Surface tension (N/m)
τ_i	Interfacial friction (N/m^2)
Δu	velocity difference of phases (m/s)
Δz	mesh spacing in flow direction (m)

Subscripts

b	boron
d	dissolved
en	entrainment
g	gas
h	isenthalpic
i	node i
$i+½$	branch after node i
$i-½$	branch before node i
is	isentropic
k	phase k (either gas or liquid)
l	liquid
m	mole
nc	non-condensable gas
r	release
sat	saturation
$stat$	static
st	stratified

1. Introduction

In analyzing various processes of energy production, the behaviour of processes in varying states must be known. Therefore, computational simulations are employed increasingly for these purposes. Especially in nuclear power plants (NPP), the accurate knowledge of the process state in various normal and abnormal situations has fundamental importance. The behaviour of NPPs in a state of emergency cannot be secured by means of small scale experiments. Therefore, the functioning of NPP processes must be modelled computationally with large computer codes. The basic part of these codes consists of the models which describe the coolant flows and heat transfer in the core. Core neutronics are simulated with one-dimensional or nowadays more commonly with three-dimensional models. The secondary side – especially steam generators, which have the strong effect on the coolability of the nuclear core – are part of the calculation model. Also, the tightness of the containment in accident situation must be ensured computationally. The development of computer technology has created new possibilities to expand and improve on the simulation models and thus respond to the new more stringent requirements of safety authorities. The codes have also been developed to be user-friendlier. In addition, some codes are currently able to simulate the entire power plant, thereby enabling their use for training purposes.

In this thesis, the six-equation model of APROS developed is described. The author has been involved in the development of this model from its first beginnings at the outset of the 1990s. The author has deducted the discretized linear equations for solving pressures, enthalpies and void fractions in accordance with the concepts shown in the reference (Siikonen, 1987). The system of constitutive equations and how equations are related to basic equations are presented and discussed in the reference (Hänninen & Ylijoki, 2005). The basic system of constitutive equations was originally conceived by Ylijoki (Ylijoki, 1991). In Publication I the author describes with how the CCFL correlations have been imple-

mented to the code and how these correlations have been verified. The later-developed non-condensable gas model and its implementation to the six-equation model are presented in the summary and in more detail in Publication II. The author has developed the higher order discretization model. It has been shown that by the aid of this model, the sharp temperature distributions can be better maintained in the liquid flow. The changes carried out to the six-equation model when applied to supercritical calculation are depicted in Publication IV. Finally, how the robustness of the complicated system is verified and how the correctness of the simulation results is validated are described and discussed.

At present, APROS is used to make safety analyses of Finnish NPPs. In the calculation of the safety analysis, only the reactor and its main cooling systems are customarily described. With APROS, however, the simulation of the whole plant including the turbine and the condenser can be modelled, and simulations can be done together with the automation system. Also, the containment can be modelled and simulated as one simulation component simultaneously with the primary circuit and the turbine plant.

1.1 Background

In the nuclear technology starting from the 1970s, the safety analysis called for thermal-hydraulic models that were reliable enough to calculate the complex phenomena related to the normal and accident situations of the water-cooled reactors. These codes were developed in many countries where the nuclear reactors were taken into use. In the USA, several versions of the RELAP-codes (Ransom et al., 1985) were developed and were gradually improved by using more detailed physical description. In France, the CATHARE (Barre & Bestion, 1995) and in Germany, the ATHLET (Teschendorff et al., 1996) codes were used for safety analyses.

In Finland, the code APROS was developed as a joint effort between VTT Technical Research Centre of Finland and Imatran Voima Oy (nowadays Fortum). It was in many respects similar to other thermal-hydraulic codes, but already from the very beginning the aim was to develop the multipurpose code. Even if the APROS is capable of simulating the reactor thermal hydraulics, it can be applied to many other processes, because in addition to thermal hydraulics, it also includes many other program packages. The extensive models for automation and electrical systems and the possibility to simulate the flue gas

flow and burning reactions enable the simulations of whole power plants – nuclear or a different type of combustion power plants.

The development of the APROS one-dimensional code was already started during the latter part of the 1980s. From the very beginning, the aim was that the code should be able to simulate the two-phase flow of the water. Due to the limited computer power, the two-phase flow and related heat transfer model was first based on the homogeneous model. In this model, the steam and water were modelled as a homogenous mixture, i.e. the steam and liquid had same temperature and they flowed with the same velocity. The main principles of this model have been presented in reference (Hänninen, 1989).

The same principles as in the homogeneous model were used in developing models for the flows of the gas mixture. In the flow and energy solutions of the flue gas, it is assumed that the flowing medium composes of gas mixture that consists of various gas components. This requires that the concentrations of the gas components in the model are solved every time everywhere along the flow network. Also, the concentration changes due to burning reactions are calculated. Even if the flue gas flow in the model is assumed to be in the gas phase, it is possible to take into account that part of the water may be in the form of liquid droplets. This happens by calculating the dew point temperature and then iterating the proportions of steam and liquid. Also, the effect of the water droplets on the flue gas mixture density is taken into account.

In the homogeneous model, the interface phenomena are omitted, i.e. there is no need to calculate the transfer of mass, momentum and heat between phases. This provides the possibility to also apply the basic equations to the two-phase flow of other fluids than water. When applying the homogeneous model to other fluids, the same type of fluid material properties as those used in the APROS water homogeneous model should be developed for the fluid in question.

Even if the homogeneous model could be used in many applications, it was clear that more sophisticated two-phase models were needed. At present, the thermal-hydraulics can be simulated with a homogeneous model, with a 5-equation drift-flux model and with a 6-equation two-fluid model. The 5-equation model is based on the separate SMABRE code (Miettinen, 1999) which is largely used for analyses of Finnish NPPs. All the models can be used in the same simulation exercise, so that the parts of the process simulated with one of the models can be connected to other parts simulated with various two-phase flow models. This thesis focuses on the six-equation part of APROS thermal hydraulics.

1.2 Six-equation model

The one-dimensional two-fluid flow model of APROS (six-equation model) simulates the behavior of a system containing gas and liquid phases. The system is governed by six partial differential equations, from which the pressures, void fractions, phase velocities and phase enthalpies are solved. The phases are coupled to each other with empirical friction and heat transfer terms which strongly affect the solution. The partial differential equations are discretized with respect to time and space, and the resulting linear equation groups are solved by the matrix equation-solving system of APROS (Juslin & Silvennoinen, 1986).

The six-equation model is based on the ideas shown in reference (Siikonen, 1987). The basics of the model were prepared already at the beginning of the 1990s, but the work in implementing new physical models and increasing the accuracy of existing models has been continued up to the present day.

Even if the numerical calculation of the flows, enthalpies and pressures in the APROS thermal hydraulic models is based on the finite difference scheme, the definition of the simulated process is made by using the process component modules and the graphical user interface. A user provides data to process components that exist in real power plants. The typical process components used in APROS are pipes, pumps, valves and heat exchangers. Also, process components specific for nuclear or combustion power plants can be used. At the same time that a user specifies the necessary data of a process component, she/he defines how many finite difference elements the process component is to be divided into. The APROS initialization program automatically creates the calculation nodalization on the basis of the process components input data and the graphically made connections between the components.

The water and steam material properties needed in simulations are interpolated using a table as a function of pressure and enthalpy. In the six-equation model, property values are separate for steam and liquid. Also, the material property values at saturation state are required (Lilja and Juslin, 1987). The problems in using the two dimensional table for the calculation of material properties are possible discontinuities. In addition, the solution system requires that the density increases monotonically with increasing pressure. After the first version of the material property table, the table points have been increased several times in order to fulfil the accuracy requirements. The material property tables have also been enlarged over the supercritical pressure area. In updating the steam and water tables, the latest data was used (International Association for

Properties of Water and Steam, 2007). Especially for values near the critical pressure point, a very dense network of the tabulated pressure and enthalpy points was needed.

The two-fluid model has also been further developed to cover the simulations of non-condensable gas flows. In this model, the non-condensable gas can be one of gases air, nitrogen, helium or hydrogen. The non-condensable gas can be as mixed with steam in the gas phase or it can be dissolved in liquid phase, and it can be transferred from one phase to another.

2. State of art

In simulation of the nuclear power plants with the system codes APROS and other similar codes like RELAP5 (RELAP5-3D Code Development Team, 2005), TRACE (Spore et al., 2000), ATHLET (Teschendorff et al., 1996) and CATHARE (Barre & Bestion, 1995), several problems are encountered. Various approaches have been developed to overcome these problems or at least to improve the results of simulations. In the following, the recent developments in simulating two-phase flow have been discussed.

2.1 Momentum transfer between phases

One of the problems in the one-dimensional two-phase flow models is the transferring of momentum between phases. The interfacial friction is very strongly dependent on the flow regime. In instances of stratified flow, the gas and liquid phases do not communicate much with each other. On the other hand, the small droplets in gas phase and small bubbles in the liquid phase flow with almost the same velocity as the bulk phase flows.

One promising approach to overcome problems in one-dimensional two-phase flow related to momentum transfer between phases is to divide the flow fields according to velocities. As an example, the annular flow usually consists of the liquid flow at the wall and of the gas flow in the middle of the pipe. At the same time, the liquid flow may include the small bubbles and the gas flow may include small droplets. These small particles flow nearly with the same velocity as the prevailing phase. In the reference (Rajamäki and Narumo, 1995), the SVAF model (Separation of the Flow According to Velocities) has been described. In this model, the momentum equations describe two fluids which consist of both phases. This kind of approach simplifies the interfacial momentum transfer models between phases, but on the other hand new types of models for the mo-

mentum transfer are needed. The present interface correlations have been developed for the system where the liquid and gas form their own mass, momentum and energy balances.

2.2 Numerical diffusion

The other problem in the one-dimensional codes based on partial differential equations is the numerical diffusion. This turns up, for instance, as a tendency to even out the sharp distributions of the solved variables. In the reference (Rajamäki & Saarinen, 1994), the shape-preserving characteristic method PLIM (Piecewise linear interpolation method) has been described. In this method, the unknown variables at mesh boundaries are represented using a piecewise linear approximation.

In the six-equation model of APROS, the numerical diffusion in liquid enthalpy calculation has been reduced by incorporating a simple higher order upwind scheme (Vihavainen et. al., 1999). The same method was also applied in solving the concentrations.

2.3 Three-dimensional phenomena

One difficulty in modelling the nuclear power plants with a one-dimensional model is the large volumes, which cannot always be modelled one-dimensionally. The one-dimensional system codes are used for the simulation of the reactor pressure vessel and steam generator secondary side, which also includes the volumes that cannot be considered as one-dimensional flow channels. Recently, various approaches have been applied to simulate the 3-dimensional two-phase flow.

One possibility to cope with the 3D problem is to add the two-phase models to existing CFD codes. The problem is that mass transfer (boiling or condensing) is difficult to properly model. One approach is that the gas inside the liquid is assumed to be always in the form of bubbles, i.e. the other flow regimes are not modelled. Realistic three-dimensional CFD modelling would need a three-dimensional net with very small calculation meshes. This would lead to the use of an extremely small time step, and consequently the computation time would be too large even for efficient modern computers.

The other approach is to add all three momentum equations to the one-dimensional system code (Glantz and Freitas, 2008). In this case, the closure

laws of the one-dimensional model with minor modifications can be applied. The problem is that the three-dimensional model only allows similar large nodes to that of the one-dimensional code. Due to large volumes any turbulence models can not properly be applied. Also, in using this approach not all the flow regimes can be simulated.

One promising approach applied to the simulation of the three-dimensional two-phase flow is a two-fluid porous media method (Stosic and Stevanovic, 2002). In this method, a control volume can be occupied by one or both phases as well as by a fraction of volume due to tube walls or rods. This way, the momentum balance automatically takes into account the fact that part of the junction is occupied by the solid structure. The conservation of liquid and gas is applied only to the fractions of control volume occupied by a corresponding phase. The advantage of the method is that it can be applied to complex geometries using relatively large control volumes. On the other hand, the effect of small details is lost in this approach.

2.4 Simulation of supercritical pressure thermal hydraulics

At present, NPPs also call for simulation capabilities in the supercritical pressure area. With the higher pressure and temperature, the efficiency of the plant can be considerably increased. Present nuclear power plants do not require such a feature, but already at this point concepts of nuclear power plants working at supercritical pressure have been designed. Safety analysis of the supercritical pressure plants require the analysis tool, which works both at supercritical pressure and at sub-critical pressure. At present, many system codes are developed in such a way that they could also be used at supercritical pressure. The APROS six-equation model already currently includes readiness for the simulation of thermal hydraulics at supercritical pressures.

One difficult problem is related to heat transfer at supercritical pressure. If the ratio of the heat flux to mass flux exceeds a certain value and the flow is upward, the heat transfer rate may suddenly be reduced and considerable heat transfer deterioration may occur. The same phenomena may occur due to acceleration. The present heat transfer correlations are unable to properly predict this phenomenon. In Jackson's new semi-empirical correlation (Jackson, 2008), the effect of both acceleration and buoyancy has been taken qualitatively into account. According to Jackson, both flow acceleration and buoyancy may exert

substantial impact in the turbulent heat transfer of the variable properties. In the following, Jackson's ideas for impairment of heat transfer in the case of acceleration and in instances of buoyancy in upward flow have been described.

When the bulk fluid enthalpy is increased due to heating, density falls. This causes acceleration of the flow in the middle of the channel, which increases the pressure gradient in the middle. Near the wall, the velocity is lower than in the bulk flow, and in this case the smaller part of the pressure difference is needed for acceleration. The excess pressure gradient aids the flow near the wall and thus reduces shear stress near the wall, and as a consequence the viscous sublayer becomes thicker and heat transfer is reduced.

In the vertical pipes, buoyancy affects the efficiency of heat transfer. The fluid is heated near the wall, and as a consequence density is reduced. In the upward flow, the force due to buoyancy near the wall aids the mean motion. The force aiding the flow reduces shear stress and may thus reduce the turbulence. This results in impairment of the heat transfer. Later on, when the flow near the wall is further affected by the buoyancy, the shear may become negative. The flow profile can become unstable, more turbulence is generated and the heat transfer is again improved. In the downward flow, buoyancy always enhances heat transfer.

3. Principles of the six-equation model

The six-equation model of the APROS code is based on the one-dimensional conservation equations of mass, momentum and energy (Siikonen, 1987). When the equations are applied to both the liquid and gas phases, a total of six partial differential equations are used. The equations observe the following form:

$$\frac{\partial(\alpha_k \rho_k)}{\partial t} + \frac{\partial(\alpha_k \rho_k u_k)}{\partial z} = \Gamma_k \tag{1}$$

$$\frac{\partial(\alpha_k \rho_k u_k)}{\partial t} + \frac{\partial(\alpha_k \rho_k u_k^2)}{\partial z} = \Gamma_k u_{ik} + \alpha_k \rho_k \vec{g} + F_{wk} + F_{ik} \tag{2}$$

$$\frac{\partial(\alpha_k \rho_k h_k)}{\partial t} + \frac{\partial(\alpha_k \rho_k u_k h_k)}{\partial z} = \alpha_k \frac{\partial p}{\partial t} + \Gamma_k h_{ik} + q_{ik} + F_{wk} u_k + F_{ik} u_{ik} \tag{3}$$

In the equations, the subscript *k* is either *l* (= liquid) or *g* (= gas). The subscript *i* refers to interface. The term *Γ* is the mass change rate between phases (evaporation as positive). The terms F and q refer to friction force and heat transfer (subscript w stands for wall). In the energy equation (3), the term *h* (solved enthalpy) is the total enthalpy including kinetic energy, i.e. $h = h_{stat} + 1/2u^2$. The potential energy is considered small and has been omitted in the energy equation.

The equations in the one-dimensional form include an unsteady term (time derivative), a convection term (space derivative) and the right-hand source term. The source term includes all the quantities that are not directly related to the basic thermal-hydraulic flow solutions, such as the heat flows from or to the solid structures (energy equation), pump head and valve/pipe wall friction losses (momentum equation). The external mass injection to the system is usually made through the mass equation convection term (as a mass flow boundary). In solving

pressures and enthalpies, the external flow is taken as constant. This same mass flow is also taken into account in the source terms of momentum equation.

The equations are discretized with respect to space and time, and the non-linear terms are linearized. In the space discretization, the staggered discretization scheme has been applied. This means that the control volumes of mass and energy are different from those of momentum. The state variables (such as pressure, enthalpy and density of both phases) are calculated in the middle of the mass mesh cells and the flow-related variables (such as gas and liquid velocities) are calculated at the border of two mass mesh cells. In solving enthalpies, the first-order upwind scheme has been utilized normally. In the mesh cell, the quantities are averaged over the whole mesh. Only in the case of stratified flow is the liquid head taken separately into account in the pressure solution.

The main idea in the solution algorithm is that the liquid and gas velocities in the mass equation are substituted by the velocities from the linearized momentum equation. In the momentum equation, the linearization has been made only for the local momentum flow. For the upwind momentum flows, the values of the previous iteration are used. In addition, the phase densities are linearized with regard to pressure. The density linearization is made using Equation (4)

$$\rho_k^n = \rho_k + \frac{\partial \rho_k}{\partial p}\left(p^n - p\right) \tag{4}$$

The superscript n refers to the unknown quantity. When this linearization is made together with eliminating phase velocities through the aid of the linearized momentum equation, a linear equation group where the pressures are only unknown variables is formed. The solving of the system requires that the density derivatives are always positive. It is also required that the phase densities obtained from the table as a function of pressure and enthalpy must increase monotonically with increasing pressure. Problems may occur especially with the liquid density. The liquid density does not change much as a function of pressure but depends more strongly on enthalpy. This feature makes it sometimes difficult to fulfil the condition of increasing density with increasing pressure. In order to fulfil this requirement, the tabulated pressure values at low pressure must be quite dense.

After the pressures have been solved, the velocities are calculated from the linearized phase momentum equations using the new pressures. The void fractions can be solved from the mass equations where the new velocities are used.

The phase enthalpies are solved using the discretized phase energy equations. For nuclear applications, the boron concentrations are solved using the mass flows of liquid. It is assumed that boron stays always dissolved in the liquid phase and that the boron effect on the material properties is omitted.

In the solution, APROS applies a method where the linear equation groups of pressures, void fractions and phase enthalpies are solved one after the other. The densities and other water material properties are updated as a function of the solved pressure and enthalpy. The solution procedure also includes the calculations of interfacial friction and heat transfer as well as the wall friction and wall heat transfer. The procedure is repeated iteratively as long as the mass errors of both phases (calculated from the mass balance equation) have been converged. The size of the convergence criterion can be defined by the user. The thermal hydraulic solution of the two-fluid system has been described in detail in the reference (Hänninen & Ylijoki, 2008).

The present solution includes the following steps:

1. The state of the pumps, valves and turbines are calculated. The calculated values are used in the source terms of momentum and energy equations.
2. Interfacial heat transfer coefficients, interfacial friction and wall friction coefficients are calculated.
3. The pressure equation is formed and pressures are solved.
4. The phase velocities are calculated.
5. The densities, saturation enthalpies and temperatures are updated using the new pressures.
6. The void fraction equation is formed and void fractions are solved.
7. Non-condensable gas distributions in gas and liquid phase are solved, partial pressures are calculated (Hänninen & Ahtinen, 2009)
8. The heat flows from heat structures are calculated and the temperatures of the heat structures connected to the flow model are solved.
9. The phase enthalpies are solved.
10. If non-condensable gas is present, the gas temperature is iterated.
11. Interfacial mass transfer rates are calculated using the interfacial heat transfer coefficients and the new enthalpies.
12. The convergence of the iteration is checked by comparing the mass errors to the maximum allowed values. If the mass error in some node is too large, the iteration cycle is repeated.

13. If the iteration has converged, boron concentrations are solved using the new state of the flow system.

After every iteration step, the gas and liquid mass errors are calculated from the gas and liquid mass equations where the calculated new values for densities void fractions and velocities are used. The user is able to define the allowed relative mass errors for both gas and liquid in each node. For larger nodes, a tighter mass error criterion should be used. Also, the maximum time step used in calculation is defined by the user. In practical cases, the maximum time step of 0.001 to 0.1 s is typically used. If no convergence problem is encountered, the relative mass error below 10^{-5} is usually achieved. If the allowed mass error criterion is not reached, the model reduces the time step to half of the presently used time step. Subsequently, the iteration is restarted from the previous (converged) time point. If the desired accuracy is not reached, the reason usually lies in very fast pressure and temperature changes which may cause large oscillating mass transfer rates between phases. The time step is not limited by the Courant criterion, but in fast transients the reduced maximum time step should be used, e.g. 0.001 s or less in large break LOCAs.

3.1 Constitutive equations

The phenomena, which depend on transverse gradients such as friction and heat transfer between the gas and liquid phases and between the wall and phases, are described in one-dimensional flow models with empirical correlations. These additional equations are needed to close the system formed by six discretized partial differential equations. The correlations are usually based on the empirical measurements and they form a complex system depending on many variables such as phase velocities, void fraction, pressure and fluid temperature, as well as saturation and wall temperatures. Because individual correlations are based on experiments made in specific test facilities, they usually cover only a limited part of the pressure, velocity, void fraction and temperature space. Therefore, various correlations for various parameter ranges are required.

In addition, the correlations are strongly dependent on the flow regime, and various correlations are usually needed for varying flow regimes. The flow regimes treated in the six-equation model are bubbly, annular, droplet and stratified flow regimes. In the code, the selection of flow regimes is based on flow velocities, steam volume fractions, rate of stratification and rate of entrainment.

In the calculations, the real prevailing flow mode usually consists of more than one individual flow regime. When the correlations are applied, the various flow regimes are taken into account using the weighting factors.

One problem in using the system of correlations is that correlations of different areas are not continuous. Therefore, the shape functions are used for the numerical reasons in transitions between correlations. These functions must be such that they ensure the smooth transition from one correlation to another.

Another problem occurs in the cases where one of the phases disappears. In that case, the friction or heat flow to the disappearing phase must be faded out smoothly. If, for instance, the heat transfer from the disappearing gas phase is too small, the phase does not disappear. In the opposite case, when the heat transfer from the tiny mass of the disappearing gas phase is large, numerical problems may arise.

In the following, the constitutive equations and how they are used in the APROS six-equation model are described and discussed (Hänninen & Ylijoki, 2005).

3.1.1 Interface heat and mass transfer

In two-phase flow, the heat and mass transfer between liquid and gas must be calculated by taking the energy flows from both phases to the interface into account. The calculation of interfacial mass transfer is then based on the requirement that the energy balance over the interface is zero. When it is assumed that the interface is in a saturated state, the following relationship is obtained

$$\Gamma = -\frac{q_{i1} + q_{ig,} - q_{wi}}{h_{g,sat} - h_{1,sat}}, \tag{5}$$

In equation (5), q_{wi} represents the heat flowing from the wall directly to the interface. The interfacial heat transfer rates are calculated separately for the liquid and gas side – q_{il} and q_{ig} respectively.

From the liquid side, the heat transfer is calculated as

$$q_{i1} = -K_{i1,}\left(h_{1,stat} - h_{1,sat}\right) \tag{6}$$

From the gas side, the interface heat transfer is calculated respectively

$$q_{ig} = -K_{ig,}\left(h_{g,stat} - h_{g,sat}\right) \tag{7}$$

Depending on the sum of heat flows, the mass transfer is either positive (evaporation) or negative (condensation).

The interfacial heat transfer coefficients K_{il} and K_{ig} depend strongly on both the void fraction and the phase flow velocities. Moreover, the various correlations must be used for evaporation and condensation. The interface heat transfer is usually strongly non-linear, and therefore the interfacial heat transfer is linearized with regard to the void fraction in solving the void fractions. In calculating the interface mass transfer rate, the under relaxation must be used, especially in the event of fast depressurization cases.

3.1.2 Interface friction, Publication I

In the six-equation model, the interface friction (friction between the liquid and gas phases) using the interface friction coefficient C_i is calculated as

$$F_i = f(\alpha)C_i\Delta u|\Delta u| \tag{8}$$

i.e. the interface friction depends strongly on the velocity difference of the phases. The function f(α) is a numerical shape function which ensures that the interface friction becomes large when either phase begins to disappear.

In the two-phase flow, the interfacial friction is strongly dependent on the prevailing flow regime. Various interfacial friction correlations are used for the various flow regimes. The modelled flow regimes are stratified flow and non-stratified flow consisting of bubbly, annular and droplet flow. The final value for the interfacial friction is then obtained as a weighted average of the various correlations. Void fraction, rate of stratification and rate of entrainment are used as weighting coefficients. With the aid of the weighting factors, the whole flow regime can be covered. The final interfacial friction is calculated using the interfacial friction of the various flow regimes and the weighing factors for stratification R and entrainment E.

$$F_i = RF_{is} + (1-R)\{(1-E)[(1-\alpha)F_{ib} + \alpha F_{ia}] + EF_{id}\} \tag{9}$$

The varying interfacial friction coefficients used in equation (9) are F_{is} for stratified flow, F_{ib} for bubbly flow, F_{ia} for annular flow and F_{id} for droplet flow. All the various interfacial friction correlations as well as weighting factors depend on the phase velocities. Therefore, the quantities have been linearized with re-

gard to phase velocities when they are used in the momentum equation. In addition, the phase velocities depend strongly on void fraction, which makes the derivation quite complicated.

Special case for the interface friction is a Counter Current Flow Limitation (CCFL). The CCFL models are based on experiments and the CCFL correlations are usually correlated by using dimensionless Kutateladze or Wallis numbers.

In the case of Kutateladze numbers, the CCFL correlations have the general form

$$K_g^{1/2} + M_n K_l^{1/2} = C_n \tag{10}$$

The variables K_g and K_l are dimensionless Kutateladze numbers for gas and liquid.

$$K_g = \frac{\rho_g^{1/2} j_g}{\left[\sigma g\left(\rho_l - \rho_g\right)\right]^{1/4}} \tag{11}$$

$$K_l = \frac{\rho_l^{1/2} j_l}{\left[\sigma g\left(\rho_l - \rho_g\right)\right]^{1/4}} \tag{12}$$

Where j_g and j_l are the superficial gas and liquid velocities, ρ_g and ρ_l are gas and liquid densities and σ is the surface tension of water.

As indicated in the reference (Freitas and Bestion, 1993), the interfacial friction coefficient C_i corresponding to Kutateladze correlation can be calculated in the form

$$C_i = \alpha(1-\alpha)\frac{Bo}{C_n^4 D}\left[\sqrt{\rho_g} + M_n^2(1-\alpha)\sqrt{\rho_l}\right]^2 \tag{13}$$

In equation (13), the Bond number is in the form

$$Bo = D\left[g\left(\rho_l - \rho_g\right)/\sigma\right]^{1/2} \tag{14}$$

The formula gives the interfacial friction in a single position corresponding to the values obtained from the Kutateladze type correlation.

The CCFL correlations are usually based on experiments performed at small-scale test facilities. At the real nuclear power plants, the dimensions of the reactor pressure vessel are very large, and therefore the downcomer and the upper tie

plate of the core call for special CCFL correlations. In the APROS six-equation model, the Glaeser CCFL correlations for a downcomer and an upper tie plate have been implemented in the code (Glaeser, 1992). The correlations are based on the downcomer and upper tie plate experiments of the UPTF (Upper Plenum Test Facility). The dimensions of the UPTF test facility correspond to the full scale, large PWR plant. The CCFL correlations for the reactor tank downcomer and for the upper tie plate of the reactor has been discussed in more detail in Publication I.

During validation, the proper coefficients C_n and M_n using the correlations were defined. The coefficients were chosen in such a way in the calculation that there was a small bias in the direction of the smaller K_l. This means that the flow downwards towards the core both in the upper tie plate case and in the downcomer case was smaller than in the experiment.

The coefficients used in APROS calculations differ from those in the original Glaeser correlations. Especially in the case of the upper tie plate, the defined coefficients were clearly smaller than the original values. In Equation (13) it can be seen that the interfacial friction depends on the void fraction in the junction formed by the holes of the upper tie plate. In the upper tie plate experiment the volumetric flow of liquid is much smaller than the volumetric flow of steam. Therefore the void fraction calculated from flows is near one. This makes the first term in Equation (13) small and consequently the smaller Kutateladze coefficient had to be used. The applicability of the used Kutateladze coefficients C_n and M_n should be validated with the data of the other large scale test facilities, but the problem is that such data is not in general available.

3.1.3 Wall friction

The wall friction calculation in two-phase flow is based on the single phase friction, which is then expanded to the two-phase area with the two-phase multipliers. The wall friction for the single phase flow is calculated as follows:

$$F_{wk} = -\frac{1}{2}\frac{f_k \rho_k u_k |u_k|}{D_H} \tag{15}$$

In equation (15), the friction factor f_k has been defined as

$$f_k = \frac{2\Delta p}{\rho u_k^2}$$

The single phase friction factor of laminar flow (low Reynolds numbers) is calculated as follows:

$$f_{sp,k} = \frac{64}{\mathrm{Re}_k} \tag{16}$$

The Blasius equation is used to calculate the single phase friction factor for smooth pipes in the turbulent area (Wallis, 1969).

$$f_{sp,k} = \frac{0.316}{\mathrm{Re}_k^{0.25}} \tag{17}$$

For smooth pipes, subscript *sp*, the maximum of the values obtained with formulas 16 and 17 is used.

If roughness is important, the Colebrook equation can be used.

For the rough pipes (subscript *rp*), the single phase wall friction factor using the original Colebrook equation is in the following form:

$$\frac{1}{\sqrt{f_{rp,k}}} = 1.74 - 2\log\left[\frac{1}{\sqrt{f_{rp,k}}}\frac{18.7}{\mathrm{Re}_k} + 2\frac{\varepsilon}{D_H}\right] \tag{18}$$

The variable ε is the relative roughness of a pipe.

As the friction factor cannot be solved explicitly from formula (18), it is used in more practical form as presented in the reference (Ransom et al., 1985).

In this approach, the approximated formula for the fully turbulent flow has been developed. In the fully turbulent flow, the Reynolds number becomes large and the friction factor is no longer dependent on the Reynolds number.

$$f_{cr,k} = \left[1.74 - 2\log\left(\frac{2\varepsilon}{D_H}\right)\right]^{-2} \tag{19}$$

The critical Reynolds number represents the state after which the flow is fully turbulent. The critical Reynolds number is calculated with equation (20) using the friction factor of equation (19).

$$\mathrm{Re}_{cr,k} = \frac{378.3}{f_{cr,k}}\left(\frac{2\varepsilon}{D_H}\right)^{-0.9} \cdot 0.355 \tag{20}$$

If the Reynolds number is less than 4000, the maximum of the laminar friction factor or the Blasius friction factor is used. Between the Reynolds number 4000 and the critical Reynolds number, the friction factor is interpolated using the Blasius equation with the Reynolds number of 4000 and the friction factor for fully developed turbulent flow. Above the critical Reynolds number, the values of equation (19) are used.

The final-phase wall friction factor is obtained by multiplying the one-phase friction factor with coefficients c_g (gas) and c_l (liquid) which take into account the effect of two-phase flow. In the calculation of these coefficients, the flow regimes are taken into account.

The purpose of the two-phase friction multipliers is to expand the pressure drop calculation of single phase flow to two-phase flow and to estimate the phase distribution on the wall of the flow channel. The multiplier is defined separately for the following flow regimes: stratified flow, non-stratified flow without droplet entrainment and non-stratified flow with droplet entrainment. The rate of stratification and rate of entrainment are used as weighting coefficients when the multiplier is calculated. For gas, the multiplier is used as

$$c_g = R \cdot c_{g,st} + (1 - R)\, c_{g,ns} \tag{21}$$

The subscript *ns* means non-stratified, *st* is for stratified flow, *ne* is for non-entrainment regime and en stands for entrainment. The coefficient R takes into account the rate of stratification and coefficient E the rate of entrainment. In the case of stratified flow the steam two-phase multiplier is taken proportionally to the perimeter occupied by the gas. In the case of non-stratified flow it is assumed that mainly liquid touches the wall. Only when the void fraction approaches to 1, the gas two-phase multiplier is taken into use. In the calculation, the liquid and steam multipliers are taken as the proportion to mass fractions.

The liquid multiplier is calculated as

$$c_l = R \cdot c_{l,st} + (1 - R)\left\{(1 - E)c_{l,ne} + E \cdot c_{l,en}\right\} \tag{22}$$

In the case of stratified flow, the liquid two-phase multiplier is taken as proportionally to the perimeter occupied by the liquid. For the non-stratified and non-

entrained flow, the mass fraction of liquid is used as the liquid two-phase multiplier. In the case of entrainment, the modified Lockhardt-Martinelli model is used for the two-phase multiplier (Lockhardt & Martinelli, 1949).

3.1.4 Wall heat transfer

The wall heat transfer consists of many separate heat transfer modes, and as a consequence the wall heat transfer must be calculated using the various correlations. In the case when the wall is hotter than the fluid temperature, the fluid is heated up through one-phase convection or through the various boiling processes. The one-phase heating to liquid or steam is calculated using the largely used Dittus-Boelter forced convection correlation. The ideas of the correlation can be found in the reference (Dittus and Boelter, 1985), which is a reprint of their original research paper. The forced convection value is compared to the natural convection heat flux, and the larger of these two is then used. The heat transfer is limited with the minimum Nusselt number 3.66, which represents the laminar convection value. The nucleate boiling is calculated using Thom correlation (Groeneveld and Snoek, 1986).

The heat transfer model of the hot wall also includes the treatment of the boiling crisis and quenching of the over-heated heat structure. In the case of the boiling crisis calculation, the definitions for wet (zone 1), dry (zone 3) and transition heat transfer zones (zone 2) are needed. The prevailing heat transfer zone is selected according to the wall surface temperature, fluid temperature, saturation temperature and void fraction. Also, the critical heat flux and minimum film boiling temperature are needed in selecting a heat transfer zone. If enough liquid water is present and the critical heat flux is more than the calculated heat flux, the wall, participating heat transfer is assumed to be wet. If the wall temperature is higher than the minimum film boiling temperature, the wall is assumed to be dry. If the critical heat flux is less than the calculated heat flux but the minimum film boiling temperature is larger than the wall temperature, it is assumed that the transition heat transfer zone is prevailing. If the heat transfer is changing from the wet zone to the dry zone, the return to the wet zone is not directly allowed, but a certain hysteresis is assumed.

Rewetting occurs when water enters an area, where the wall temperature is above the minimum film boiling temperature. The quench front position is on the elevation of the boundary between the wetted and dry or transition heat transfer zones. The heat transfer is enhanced above the quench front due to the

dispersed droplet cooling. The quenching process ejects droplets and thus the flow is accelerated, increasing the heat transfer rate (Clement & Regnier, 1978). If the quenching front propagates downwards, the heat transfer enhancement is not calculated. In order to be able to better simulate the rewetting phenomena, the heat conduction inside the wall should be calculated two-dimensionally (in radial and axial directions). In this case, a dense nodalization also in axial direction should be used.

When the heat transfer zone is 3 (dry wall), heat transfer is calculated between the wall and the gas phase. The zone 3 is prevailing either when the heat transfer is higher than the critical heat flux (Departure from nucleate boiling, DNB) and the wall temperature is higher than the minimum film boiling temperature or when the fluid includes very little liquid water (Dry out). In the case of DNB the Berenson correlation (Berenson, 1961), is used for pool boiling which is dominant for low void fractions and low mass flows. In the case of dry out, the Dittus-Bolter correlation for steam flow is applied.

In the case when the wall is colder than the fluid, the fluid is cooled down through one-phase convection or through condensation heat transfer. In the case of condensation, the heat transfer is calculated either with Shah, Chen or with the correlation, which is based on Nusselt theory on falling film of condensate flow. In calculating the condensation, the orientation of the heat structure must be taken into account. Also, the condensation occurring inside or outside a pipe as well as the condensation occurring on tube banks are considered in the condensation model.

3.2 Non-condensable gas model, Publication II

In the two-fluid APROS model, the treatment of non-condensable gases has also been included. In the present model, it is assumed that there is only one non-condensable gas present in the simulated system at a time, but a user can choose between four different gases. The simulated gases are air, nitrogen, helium and hydrogen. For each gas, the necessary material properties are calculated as a function of temperature. The gas density is calculated using an ideal gas equation.

In this model, the non-condensable gas can be either a part of the gas phase or it can be a dissolved component in the liquid phase.

In the gas phase, the non-condensable gas and the steam form the homogeneous mixture, i.e. they have the same temperature and the same velocity. The non-

condensable gas density in the gas phase is solved after the pressures, velocities and void fractions have been solved.

In the dissolved gas model of the six-equation model, the maximum concentration of the dissolved gas as a function of pressure and temperature is calculated. On the basis of the maximum and the real concentration, the model calculates the released gas flow. This released gas is then taken into account in the gas phase solution and in the concentration solution of the dissolved gas.

If the maximum concentration is larger than the real concentration, and at the same time the gas phase includes a considerable amount of non-condensable gas with higher gas partial pressure than the corresponding partial pressure of dissolved gas, the gas is gradually dissolved and the small gas flow from gas to liquid is calculated.

3.2.1 Non-condensable gas density, pressure and gas temperature

In the following, how the solution of the non-condensable gas is related to the pressure flow solution of the six-equation model is presented. The mass equation for the non-condensable gas is

$$\frac{\partial(\alpha_g \rho_{nc})}{\partial t} + \frac{\partial(\alpha_g \rho_{nc} u_g)}{\partial z} = \dot{m}_r \tag{23}$$

In equation (23), the subscript g refers to the gas mixture and nc refers to non-condensable gas. The variable $\dot{m}_r$ is the released or dissolved mass flow/volume of a non-condensable gas. For the numerical solution, the partial differential equation (23) must be discretized with regard to time and space. The following linear equation is obtained (Hänninen & Ahtinen, 2009):

$$a_i \rho_{nc,i}^k = a_{i+1} \rho_{nc,i+1}^k + a_{i-1} \rho_{nc,i-1}^k + b_i \tag{24}$$

In equation (24), the following abbreviations have been used:

$$a_i = V_i \frac{\alpha_{g,i}}{\Delta t} + A_{i+1/2} \alpha_{g,i+1/2} \left[u_{g,i+1/2}, 0 \right] + A_{i-1/2} \alpha_{g,i-1/2} \left[-u_{g,i-1/2}, 0 \right] \tag{25}$$

$$a_{i+1/2} = A_{i+1/2} \alpha_{g,i+1/2} \left[-u_{g,i+1/2}, 0 \right] \tag{26}$$

$$a_{i-1} = A_{i-1/2}\alpha_{g,i-1/2}\left\lfloor u_{g,i-1/2},0\right\rfloor \tag{27}$$

$$b_i = V_i \frac{\left(\alpha_g \rho_{nc}\right)_i^{t-\Delta t}}{\Delta t} + V_i \dot{m}_r \tag{28}$$

In equations 24 to 28 the branch void fractions are calculated as upwind values, i.e. using the values of the node where flow comes from.

In the solution of the total pressure, the gas density derivative with regard to the pressure is used. When the non-condensable gas is present in the gas phase, the density derivative of gas is calculated as follows

$$\frac{\partial \rho_g}{\partial p_g} = x_{m,nc}\left(\frac{\partial \rho_{nc}}{\partial p_{nc}}\right)_{is} + \left(1 - x_{m,nc}\right)\left(\frac{\partial \rho_s}{\partial p_s}\right)_h \tag{29}$$

The density derivative of non-condensable gas is calculated from the isentropic gas equation, i.e.

$$\frac{\partial \rho_{nc}}{\partial p_{nc}} = \frac{M_{nc}}{\gamma RT} \tag{30}$$

The mole fraction of non-condensable gas $x_{m,nc}$ is calculated with the formula (31).

$$x_{m,nc} = \frac{\rho_{nc}}{M_{nc}} \Big/ \left(\frac{\rho_{nc}}{M_{nc}} + \frac{\rho_s}{M_s}\right) \tag{31}$$

After the total pressure of gas p_g has been calculated, the partial pressures can be calculated by utilizing the mole fraction of the non-condensable gas.

After the gas total enthalpy and steam and gas densities have been solved, the gas temperature can be iterated, using the condition that after the solution of the total gas energy the following energy balance equation must be valid

$$\rho_g h_g\left(T_g\right) = \rho_s h_s\left(T_g\right) + \rho_{nc} h_{nc}\left(T_g\right) \tag{32}$$

3.3 Dissolved non-condensable gas

The purpose of the model is to simulate the amount of non-condensable gas that may be released from the liquid phase to the gas phase as a consequence of the pressure decrease. Also, the slow dissolution of the gas to the liquid phase is taken into account. The release of gas is usually much faster than the dissolving process. In the release process, numerous bubbles are formed on the wall. These bubbles are detached from wall and coalesced and they start to flow upwards. In the dissolution process, the interface area between liquid and gas is usually small (stratification), and as a consequence the process is slow. In the reference (Sarrette, 2003), the modelling of release and dissolution is described.

At the moment, the effect of dissolved non-condensable gas on the liquid density is omitted, due to the fact that the density increase resulting from the dissolved gas is small. The amount of the dissolved gas at the initial state is defined using a parameter that defines the proportion of given dissolved gas to the maximum amount.

In the model, the maximum concentration of the dissolved non-condensable gas as a function of pressure and temperature is calculated. On the basis of the maximum and the real concentration, the six-equation model calculates the released gas flow. If the real concentration is larger than the maximum concentration, the released nitrogen mass flow is

$$\dot{m}_r = \left(x_d - x_{\max}\right)\left(1-\alpha\right)\rho_l / \tau_r \tag{33}$$

In the formula (33), x_d is the mass fraction of dissolved gas, x_m the maximum mass fraction of dissolved gas, τ_r the time constant for dissolved gas release and Δt the time step.

If the maximum concentration is larger than the real concentration and, at the same time, the gas phase includes a considerable amount of non-condensable gas (high gas partial pressure), the gas is gradually dissolved and the small gas flow from gas to liquid is calculated.

$$\dot{m}_d = \left(x_d - x_{\max}\right)\alpha\left(1-\alpha\right)\rho_n / \tau_d \tag{34}$$

In equation (34), $\dot{m}_d$ is the dissolving mass flow/volume ($\dot{m}_r = -\dot{m}_d$ in equation 33), ρ_{nc} is the non-condensable gas density, τ_d the time constant for dissolution.

The solution of the dissolved gas mass fraction is based on the mass balance of liquid.

$$\frac{\partial((1-\alpha)\rho_l x_d)}{\partial t} + \frac{\partial((1-\alpha)\rho_l u_l x_d)}{\partial z} = \dot{m}_d \qquad (35)$$

The dissolved mass fraction distribution is solved using the standard APROS matrix solver.

The release or dissolving mass flows of the non-condensable gas are taken into account in the void fraction solution, the mass balance of gas phase, the energy balance of the gas phase, the mass balance of dissolved gas, the energy balance of the liquid phase and the calculation of mass errors. The non-condensable gas model has been tested and validated. It works robustly and it does not excessively increase the simulation time.

3.4 Higher order upwind discretization scheme for liquid enthalpy model, Publication III

In the APROS six-equation model, solved quantities such as phase enthalpies and concentrations are calculated using the first-order upwind scheme. In this scheme, the average value of the solved quantity is used in the convection term, i.e. the flow out of the mesh cell transports all the time the quantity with the average value. The drawback of the method is that sharp distributions of solved quantities are non-physically smoothened, when the fluid flows ahead over calculation meshes. The phenomenon can be attenuated by using dense nodalization and small time steps, but the problem cannot be fully eliminated.

Due to this numerical diffusion, the accurate simulation of thermal stratification is not possible using the first-order discretization. In the six-equation APROS model, the author modified the discretization of the liquid enthalpy model. The model was improved by adopting a simple higher order upwind scheme capable of decreasing the numerical diffusion over the sharp layer of the hot and cold water in vertical tanks. This model has been described in Publication III (Vihavainen et. al., 1999). For the validation of the model, experimental data from VTT's PACTEL experiments with a passive core make-up tank was calculated (Purhonen et al., 2006).

3.4.1 Modified discretization of the liquid energy equation

The main idea in the higher order upwind model is to use the values of three nodes for defining the distribution function for the out-flowing liquid enthalpy. In this model, the transported liquid enthalpy h_x is defined with three latest iterated liquid enthalpies $h_{l,i}$, $h_{l,i-1}$ and $h_{l,i+1}$, and h_x is calculated as follows:

$$h_x = h_{l,i+1} + f(h_{l,i-1}, h_{l,i}, h_{l,i+1})(h_{l,i-1} - h_{l,i+1}) \qquad (\text{if } u_l > 0) \qquad (36)$$

or

$$h_x = h_{l,i-1} + f(h_{l,i-1}, h_{l,i}, h_{l,i+1})(h_{l,i+1} - h_{l,i-1}) \qquad (\text{if } u_l < 0) \qquad (37)$$

With the aid of the function f, the desired behaviour for the change of the enthalpy to be transported from node i is obtained (in the case $u_l > 0$, $h_{l,i}$ is changing from $h_{l,i+1}$ to $h_{l,i-1}$, and in this case, $u_l < 0$ $h_{l,i}$ changes from $h_{l,i-1}$ to $h_{l,i+1}$). The idea in choosing a proper function was to find the sort of function that delays the change of the upwind enthalpy. Various alternatives for function f were tested, and the power function with exponent 4 was simply selected. The power function is continuous, it delays enthalpy transition sufficiently and did not cause any numeric problems (see Figure 1).

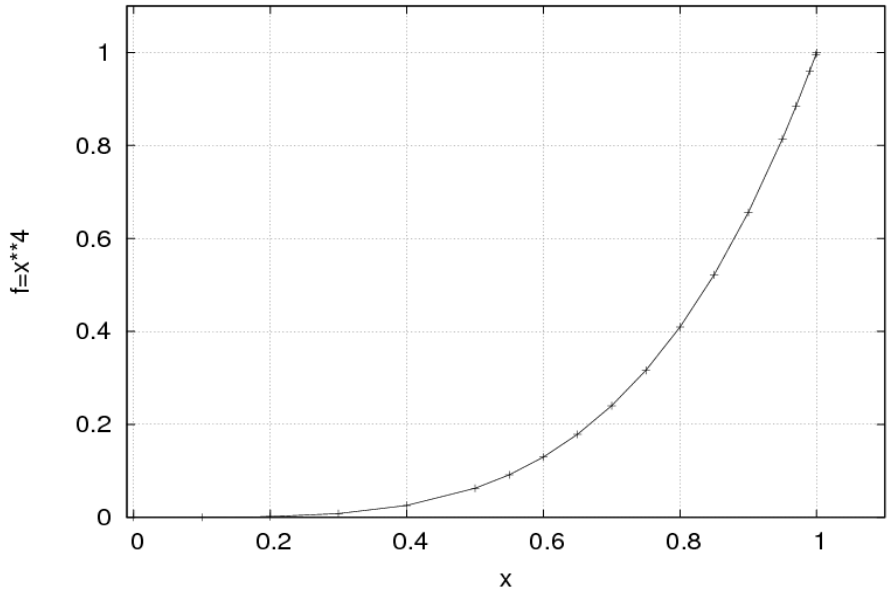

Figure 1. Behaviour of function x^4, when $0 < x < 1$.

In the case when $u_l>0$, the following function is used:

$$f = \left[\frac{h_{l,i} - h_{l,i+1}}{h_{l,i-1} - h_{l,i+1}} \right]^4 \tag{38}$$

The function f changes from 0 to 1 when the enthalpy $h_{l,i}$ changes from $h_{l,i+1}$ to $h_{l,i-1}$. In the case when $u_l < 0$, the following function is used:

$$f = \left[\frac{h_{l,i} - h_{l,i-1}}{h_{l,i+1} - h_{l,i-1}} \right]^4 \tag{39}$$

The function f changes from 0 to 1 when the enthalpy $h_{l,i}$ changes from $h_{l,i-1}$ to $h_{l,i+1}$. Because the transported enthalpy is a solved quantity, the equations (36) and (37) cannot be used directly in the enthalpy solution. The desired enthalpy change is obtained by manipulating the convective term in the liquid enthalpy equation. In the case of positive flow, the convective term of junction *i+1/2* is modified as

$$\frac{h_x}{h_{l,i}} A_{i+1/2}\left((1-\alpha)\rho\right)_{i+1/2} u_{i+1/2} h^n_{l,i} \tag{40}$$

where h_x is calculated from the equation (36) or (37) and $h_{l,i}$ is the latest iterated enthalpy.

The new model is applicable for simulation of thermal stratification in vertical pipes and tanks, such as the passive core make-up tank or conventional hot water storage tanks. It can also be used for simulation of a hot or cold water pulse in a horizontal or vertical pipeline. The developed model is able to handle positive and negative enthalpy changes and the flow direction may change during simulation. The user must define the flow path where the sharp enthalpy change is to be followed, i.e. where the new discretization scheme is used. Otherwise, the normal pure upwind scheme is used. Each node should be connected only to two junctions where the modified upwind calculation scheme is applied, but one node can be connected to several ordinary junctions without the higher order discretization treatment. The model presumes that the distribution does not proceed through a whole calculation node in the one time step, i.e. $v < \Delta l/\Delta t$. Even if the new model considerably improves the treatment of the sharp temperature distribution, the real sharp distribution is maintained only if sufficiently dense nodalization is used. This is partly because the temperature is calculated as a function of the solved enthalpy $h_{l,i}$, which still represents the average enthalpy of a node.

The concentration transport equation has the same form as the liquid enthalpy equation and the model therefore has also been applied to solve the concentrations of liquid flow. Especially solving the boron front propagation, the model has practical meaning in analysing the reactivity transients.

3.5 Supercritical pressure flow model, Publication IV

Fossil-fuelled power plants have been operated with water at supercritical pressures for decades due to the high thermal efficiency achievable by increasing the system temperature and pressure above the critical point. In recent years, there has also been increasing interest in developing water-cooled nuclear reactors which work above the supercritical pressure conditions. When such reactor concepts are studied, it is necessary that the simulation codes are also able to simulate water flows above the critical pressure. At the moment, the nominal pressure of the new PWR type power plants is about 160 bar. It is thus quite realistic to

expect that, in some transients, the supercritical pressure may be achieved. Consequently, the simulation capabilities at supercritical pressure area may be needed for the present NPPs. APROS was one of the first system codes where the six-equation model was extended to the supercritical pressure calculation.

3.5.1 Description of APROS model

At supercritical pressures, the distinction between the liquid and gas phases disappears: boiling and condensation are not observed, but instead the properties of the fluid vary smoothly from those of a liquid-like fluid to those of a gas-like fluid. From the macroscopic point of view, the supercritical-pressure fluid can always be considered a single-phase fluid. Therefore, the homogeneous model would be ideal for the thermal hydraulic simulation at and above the critical pressure. However, in nuclear power plant applications, the homogeneous model is seldom sufficient for the calculation of two-phase flow below the critical pressure, and thus the six-equation model must be used under general conditions.

When the six-equation model is applied to supercritical-pressure calculation, problems with regard to how the model behaves near and above the critical pressure and how the phase transition through the supercritical-pressure region is handled are inevitably encountered. Above the critical pressure, the heat of evaporation disappears, and the whole concept of phase change is no longer meaningful. The set of constitutive equations needed in the six-equation solution includes friction and heat transfer correlations developed separately for both phases. The capability of constitutive equations and the way they are used must be carefully examined.

One particular problem encountered is due to the water and steam material properties. Especially for values near the critical pressure point, a very dense network of the tabulated pressure and enthalpy points was needed. The heat capacities of the liquid and steam approach to infinity simultaneously with the latent heat of evaporation approaching zero. These difficulties can usually be overcome by limiting the values to a certain finite sensible value.

In the present APROS six-equation model, the pseudo liquid and gas phases have been maintained. In the supercritical model, the concept of the pseudo-critical line is used to define the state of fluid. The pseudo-critical line is an extension of the saturation curve to the supercritical pressure region: it starts from the point where the saturation curve ends (the critical point), and it can be thought to approximately divide the supercritical pressure region to sub-regions

of pseudo-liquid and pseudo-gas; for at the same point where c_p is maximized, the variation of density ρ as function of temperature is also steepest (see Figure 2).

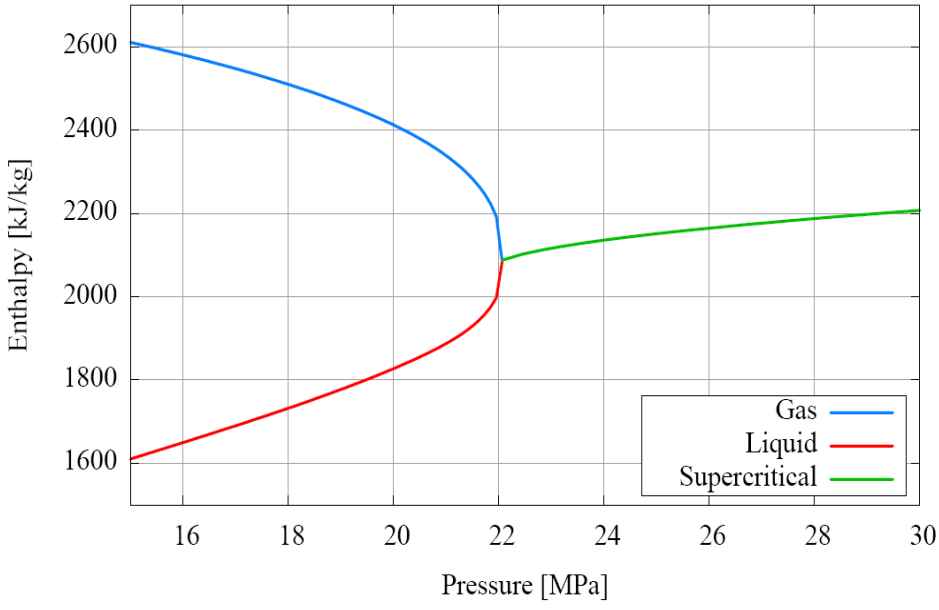

Figure 2. Saturation enthalpies of steam and liquid at sub-critical pressure and pseudo saturation enthalpy at supercritical pressure (Hänninen & Kurki, 2008).

In order to preserve separate liquid and gas phases in the model, a small evaporation heat is assumed at the pseudo-critical line. Using minimal evaporation heat, the phase change from liquid to gas can be calculated using the normal mass transfer formula. In this model, if the enthalpy is above the pseudo-critical line, the fluid consists of gas; whereas if enthalpy is below the pseudo-critical line, the fluid consists of liquid. The interface heat transfer coefficients are kept large enough to ensure rapid transition from liquid to gas and vice-versa. The thermo physical properties of water/steam undergo rapid changes near the pseudo-critical line, and therefore the quality and accuracy of the steam tables are essential in calculating the flows at supercritical conditions. The steam tables used in APROS are based on the IAPWS-IF97 recommendation. The new steam table defines the properties of water with a sufficient accuracy over a wide range of parameters, including supercritical pressures.

The changes made in the constitutive equations of the APROS two-fluid model have been discussed in Publication IV. The applicability of the numeric

model is demonstrated by simulating instant emptying of a horizontal pipe, i.e. Edward's pipe experiment initially at supercritical pressure. Several cases with various initial conditions are calculated and discussed. The calculation of the wall-to-fluid heat transfer is examined with a model of supercritical water flowing through a heated pipe.

The six-equation model thermal-hydraulics model has been used to simulate the High Performance Light Water (HPLWR) -reactor concept developed in the EU-project (Kurki & Seppälä, 2009). In this concept, the cooling flow is through path, which goes three times through the core – two times up and once down. In particular, the heat transfer calls for the well validated the heat transfer correlations.

3.5.2 Heat transfer at supercritical pressure

The heat transfer at the supercritical pressure differs from the heat transfer in the sub-critical pressure area. The Dittus-Boelter type heat transfer correlations may predict the heat transfer rate quite well if the heat flux/mass flux is not very large. The heat capacity near the critical point increases considerably, which increases the Prandtl number and hence the heat transfer coefficient. However, if the ratio of the heat flux to mass flux exceeds a certain value and the flow is upward, the heat transfer rate may suddenly be reduced and considerable heat transfer deterioration may occur. The material properties of fluid (density, viscosity, heat capacity) usually undergo rapid change near the pseudo-critical line. In the correlations, this change is taken into account by calculating the material properties both at wall temperature and at the fluid bulk temperature, and then the ratio of the property at two temperatures is used in the correlation. The wall friction in the APROS two-fluid model is calculated with the correlation of Kirilow (Pioro et al., 2004). In this correlation the fast density change due to temperature is taken into account.

In the two-fluid model of APROS, the heat transfer correlation of Bishop (Bishop et al., 1965), as well as the correlation of Jackson and Hall (Jackson and Hall, 1979) is used above the critical pressure area. These correlations predict heat transfer quite well when the heat flux ratio to mass flux is not very large, but they do not predict the impairment of the heat transfer in upward flow. The impairment of heat transfer can be caused as a result of acceleration or buoyancy, or both.

4. Validation and application of the six-equation model

The six-equation model forms of a complex system of six linearized and discretized partial differential equations, empirical correlations and steam and liquid material properties. The six-equation model and other models of APROS are being gradually developed on a continuous basis, and the new features are adopted in new APROS versions. In order to ensure the right function of the code, the continuous validation of the system is needed.

In the following, the developmental assessment of the six equation model has been shortly described. Also, simulations of selected important integral tests and real plant cases have been depicted.

4.1 Developmental assessment

When new correlations or other models are implemented in the six-equation model or in other parts of APROS, a certain procedure must be performed. The new model is verified by the person who has made and programmed the model in APROS. This verification includes an adequate number of tests which ensure that the new model functions as expected under various circumstances. The new feature is properly documented in the APROS documentation. It is particularly important to describe what changes have been done and why these changes have been made. Each time a new version of APROS is released, the list of changes made for the new version is also provided. This is important to ensure the traceability of changes.

Purpose of the validation is not only to see that the correlations provide realistic values but also to ensure cooperation between correlations. The problem in using the system of correlations is that the various correlations are not continuous. Varying correlations are needed for varying flow regimes. In heat transfer,

various correlations are needed, depending on the heat transfer mode. Therefore, in transitions between correlations, shape functions are used for numerical reasons. These functions have to be such that they ensure the smooth transition from one correlation to another.

In validation of the APROS two-fluid model, three varying categories of test cases have been used. The individual correlations have been validated using separate effect tests. These are the tests which have been performed at simplified test facilities. The advantages of these tests are that certain properties can be measured accurately, and the comparison between calculated and measured values can subsequently be carried out reliably.

The integral test facilities are those that simulate the larger systems: often these are small-scale models of real plants. These can be used to validate how the simulation model is able to predict the behaviour of the whole plant system. The advantage of these tests is that the necessary quantities for the comparison can be measured. The disadvantage is that the scale effects cannot be confirmed.

The best tests would be real plant transients, but due to high requirements on plant safety, tests cannot be carried out on an intentional basis. Also, due to the high reliability of plants, plant incidents are rare.

In the following, the validation using different types of test cases is described. The validation of the APROS two-fluid model includes many more cases, but here a selected part of the cases has been chosen to describe the principle of continuous validation work. The new features described in the dissertation, such as supercritical pressure and non-condensable gas calculations, are not yet a part of continuous validation, but the proper tests will be included in the validation procedure. The applications calculated with APROS are also briefly described.

4.1.1 Separate effect tests

In the validation procedure of the new versions of APROS, certain separate effect tests are calculated each time a version is released. In the following, some of these tests are described (Ylijoki et al., 2008).

4.1.1.1 Interface correlations, rapid depressurization

The purpose of the Edwards pipe test is to examine the phenomena related to sudden depressurization of a horizontal pipe. The Edwards pipe test facility (Edwards and O'Brien, 1970) is a horizontal pipe closed at the beginning of the

test, which contains water under high pressure (6.895 MPa). The initial water temperature is 242 °C. The length of the pipe is 4.096 m and diameter 0.073 m. One end of the pipe is punctured, after which water begins to evaporate and flow out of the tube under high velocity. At the very beginning of the test, the pressure in the pipe decreases rapidly and subsequently it stays almost constant. After about 0.25 seconds, the decrease becomes steeper until the pressure finally drops to the air pressure. During the test, the state of the fluid changes from 70 bar liquid to 1 bar steam, i.e. it covers a large area from one-phase liquid through two-phase flow to steam flow. Therefore, the test reveals possible deficiencies and coding errors in the interface heat transfer well, together with interface friction correlations and wall friction correlations. Also, this test has indicated the misbehaviour of steam and water material properties on several occasions. In Figure 3, the measured and calculated pressures near the closed end of the APROS six-equation model have been compared.

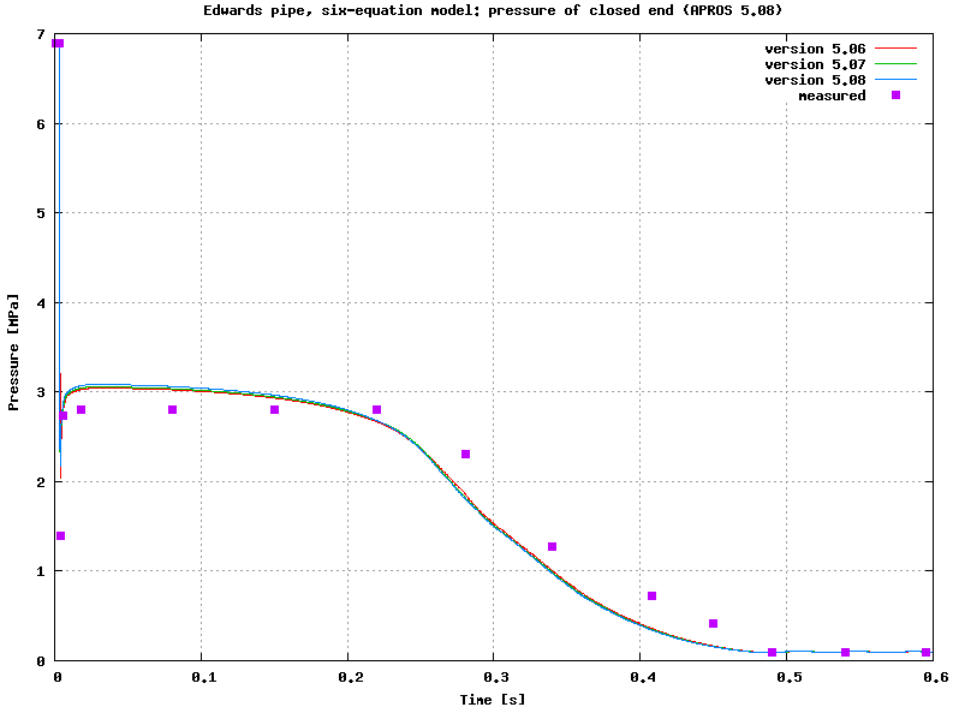

Figure 3. Calculated and measured results of the Edwards pipe: pressure at closed end of pipe.

4.1.1.2 Top blowdown experiment

The Battelle top blowdown experiment (Hölzer, 1977) is the test for the rapid depressurization for the vertical system. This experiment demonstrates the rise of water level in a boiling water reactor in the event that the pressure is suddenly decreased. In particular, the interface friction correlations in the vertical flow channels affect the calculation results. Because the flow through the discharge valve is critical most of the time, the critical flow models of the six-equation model for steam and two-phase flow are tested. The test vessel has an inner diameter of 0.77 m and a height of 11.19 m. The initial pressure is 7.07 MPa, temperature 285 °C and height of water level 7.07 m. At the beginning of the test, a break orifice in the discharge nozzle (at the height of 10.01 m) is opened. The area of the orifice is 0.064 m. The nozzle is modeled with a small node.

When the break orifice is opened, the water level begins to rise. When the level rises to the discharge height, the total break flow, because of the greater amount of liquid water, increases sharply. The calculated mass flow begins to increase almost at the right time and the maximum flow is a little higher than in the measurements. The more calculation nodes are used, the sharper the increase becomes. In Figure 4, the measured and calculated discharge mass flows of the APROS six-equation model have been compared. In version 5.08 (Ylijoki et al., 2008), the critical flow model of the steam was modified, and as a consequence the water level reaches the discharge level earlier than in calculating with earlier versions.

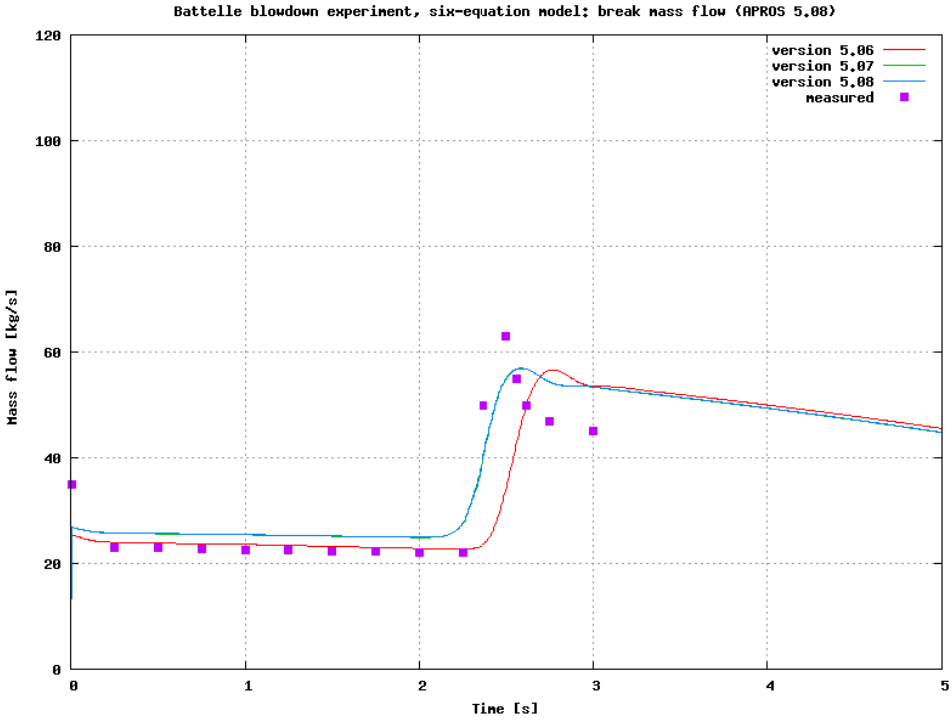

Figure 4. Calculated and measured results of the Battelle blowdown experiment: break mass flow.

4.1.1.3 Wall heat transfer tests

The wall heat transfer must be tested by means of several tests. The Becker experiments (Heat Transfer Correlations in Nuclear Reactor Safety Calculations, 1985) have been used to test the heat transfer correlations for dry out and post dry out at steady state conditions. The test section is a vertical tube filled with water at the beginning of the test. The wall of the tube is directly heated with a uniform power distribution and the tube is insulated on the outer surface. The inside diameter of the tube is 0.0149 m and the heated length 7 m. Water flows into the system at a constant rate from below.

The experiments have been calculated by dividing the tube into 100 nodes and into corresponding number of heat structures. The boundary conditions were defined by an external branch with the desired mass flow into the system and an

external node with the correct exit pressure. The tests were carried out by simulating the system until it reached a steady state. This took about 50–100 seconds of simulation time. In the case calculated, pressure was 2.98 MPa, inflow mass flux was 498 kg/m^{2}s, sub-cooling 8.9 °C and heating rate 0.562 MW/m^2.

A dry out phenomenon occurs in the upper part of the tube, i.e. where the heat flux exceeds the critical heat flux. A sharp increase in the wall temperature distribution is noticed on the border of the wetted and dry wall. The height of the border in the calculation results is quite close to that obtained in the measurements. However, the shape of the distribution differs somewhat above the border. In general, the point for the dry out position was difficult to predict. In the case shown in Figure 5, the position was well calculated, but in some other cases the calculated position for the dry out was clearly too high. In the present calculation, the critical heat flux was simulated with Biasi correlation. The calculation results of this experiment are sensitive to changes in heat transfer models. The results using version 5.08 were changed compared to those of previous versions, because the discretization in heat conduction calculation was slightly modified.

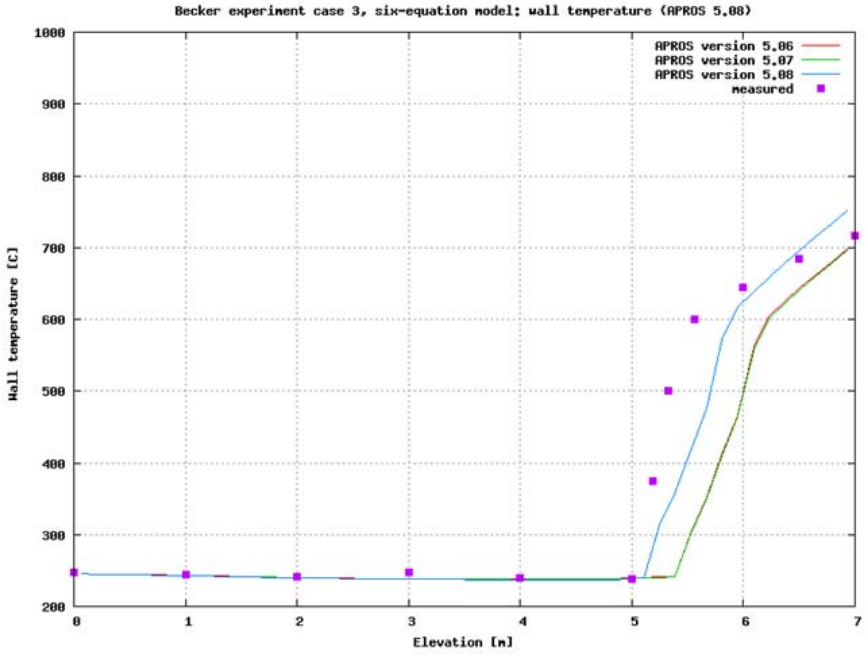

Figure 5. Calculated and measured results of Becker's experiment: wall temperature at various elevations inside the heated pipe.

One of the important applications where APROS is used is the simulation of LOCA accidents. Especially in large break LOCAs of PWRs, the core is overheated and reflooding and quenching phenomena are encountered. For the validation of the APROS reflooding models, the ERSEC reflooding test is used (Deruaz & Tellier, 1979). In this experiment, the 3.325 m long pipe – which has a constant initial temperature 600 °C and a constant heating 6267.5 W – is cooled down by injecting water at 23 °C with a constant mass flux of 52 kg/s/m^2 to the bottom of test section. The transient was simulated by means of the simulation model, where the heated pipe was divided into 500 nodes. A dense nodalization is needed due to special models used in the vicinity of the quench front. In this type of transient the axial heat conduction must be calculated. The axial temperature distribution is needed to find the quench front position. Also the axial temperature gradient near the quench front is needed to enhance the quench front propagation. In Figure 6, the calculated and measured quench front propagation rates are compared to each other. The simulated behaviour of the experiment is quite close to the measured values. At the beginning of the experiment, the simulated quench front moves somewhat too fast, and at the end of the experiment too slowly. Above the quench front the heat from the wall is transferred only to steam. At the end of transient the steam temperature at outlet was too high. At the same time the liquid flow out was higher than the measured flow. This implies that liquid droplets do not cool steam sufficiently, i.e. heat transfer between phases was too small

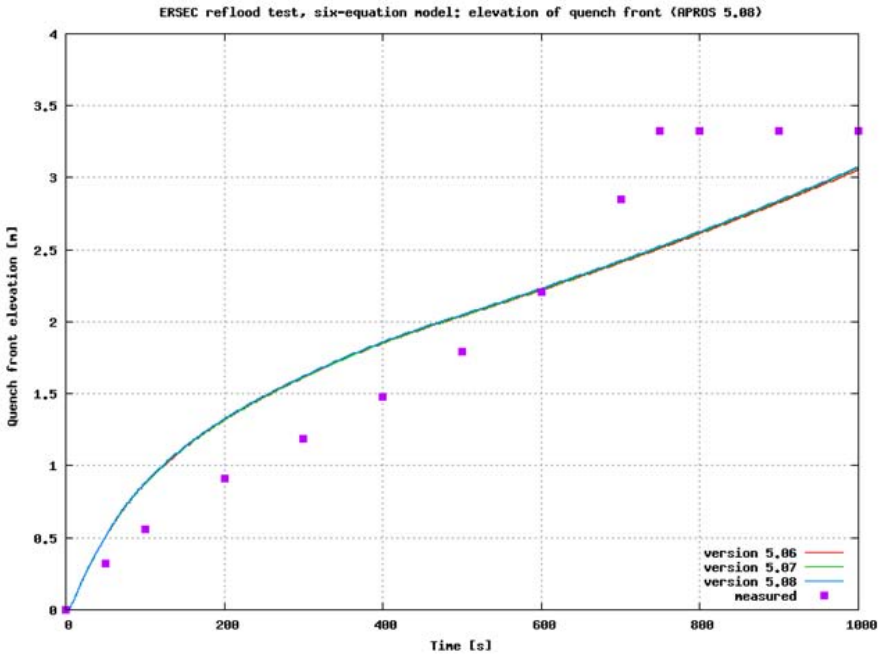

Figure 6. Calculated and measured results of ERSEC reflooding test: propagation of quench front.

4.1.2 Testing with power plant models

As part of continuous validation, some power plant transients are also calculated. The APROS six-equation model has been used for the simulation of Finnish nuclear power plants in Loviisa (VVER) (Puska and Porkholm, 1991) and in Olkiluoto (BWR) (Norrman, 1995 and Ylijoki, 2003), and therefore the proper models of these plants are available for validation. The model of Loviisa consists of all major systems of primary and secondary circuits. Also, the most important part of the automation system has been modelled. The simulation model of Olkiluoto includes the reactor core and tank with main components, steam lines and feed water lines up to the turbine and dump valves. The auxiliary systems and controllers of plant have been modelled to the extent needed for typical safety analyses.

During the development assessment, the Loviisa model is used to calculate two transients – the stopping of one recirculation pump and the reactor trip. The calculated values are compared to the measured values. The validation cases of

the Olkiluoto model are the steam-line break and the reactor trip. The calculated values are compared with the results calculated by means of the Goblin code (Mitchell and Zhao, 1996).

4.2 Integral tests

The partial differential equations, correlations, steam properties and process component models (valves, pumps, turbines and heat exchangers) form a complicated system that must be validated together. Therefore, in addition to separate effect tests where only one part of the correlations is tested, the integral tests are important to validate how the various correlations work together in the whole two-fluid model. The PACTEL-test facility simulating the VVER-440 plant has been a valuable tool for validating the APROS two-fluid model. In the reference (Plit et al., 1997), the small-break LOCA experiments of the PACTEL test facility have been simulated with the APROS two-fluid model. In the small-break experiments, the main problem is related to the liquid water distribution in the test facility. In particular, the amount of liquid water in the loops affects how well the core can be cooled. In this case, the results correspond well to the measured values. This kind of testing also proves the accuracy of the nodalization that should be used in various parts of the test facility.

4.3 Validation with a real nuclear power plant transient

Due to the high safety level required for real nuclear power plants, there are usually no real plant transients available for validation. One real plant transient simulated with the APROS six-equation model was a transient in which the turbine-by-pass valve of the Loviisa 2 was stuck open (Puska et al. 1994). In this transient, the measured data and operator actions were available, and a sensible comparison between the calculated results could be performed. The calculated results and the measured data in general correspond well with each other. The simulation of this transient also proved that, in order to be able to simulate real power plants, the whole system of the plant including all essential automation systems must be modeled.

4.4 Applications for real plants

The main application that the developed model is intended for is to prove that the NPPs behave safely in unexpected events. Examples for these kinds of events are the various sizes of LOCAs, various sizes of secondary leakages, leakage from the primary to the secondary side, disturbances in steam pressure or flow and disturbances in feed water flow or feed water temperature. Often the loss of off-sidepower is assumed to take place simultaneously with these events. Safe behaviour should be shown not only for new NPPs but also for NPPs that have been in use for many years, especially if the power is upgraded or some other major modifications are performed at the plant. A typical example of safety analysis procedures is shown in the reference (Plit et. al 2000). In the paper, the safety analysis calculations using the APROS code performed for the Loviisa NPP in the connection of the modernization and power upgrading are described and discussed.

In addition to Finnish companies and organizations, APROS is utilized at present in about 20 countries. Both in the combustion and nuclear power plant code packages of APROS, the six-equation two-phase model is the main tool for thermal hydraulic simulations.

5. Conclusions

In the dissertation, the two-fluid model has been described to such extent that the basics of the APROS six-equation model can be understood. The main goal in this presentation is to prove that the whole complicated two-fluid model with the constitutive equations, aided by the non-condensable gas model, can be used for the various analyses of NPPs.

An important part of the two-fluid system is constitutive equations needed to close the system of partial differential equations. Most correlations are based on the small scale tests, and their ability to predict large-scale phenomena is not always sufficient. The Glaeser CCFL correlations implemented in the APROS six-equation model are based on the full-scale experiments of the UPTF test facility.

In the thesis, it has been shown that with the aid of the new discretization model the sharp distribution of hot and cold water in tanks can be maintained, even if in this case it did not have much effect on the overall course of transient. The same higher order discretization model has also applied for the boron concentration simulation. The possibility to follow the propagation of the boron front in the primary circuit is very important in analyzing reactivity transients.

In the power plants, the non-condensable gases can be present in two-phase flow, and often they may affect the behaviour of the processes. Especially in emergency situations of NPPs, the effect of the gases must be known. The implemented non-condensable gas model of APROS also includes the treatment of the dissolved gas. This feature is needed especially when emergency cooling water is injected into the primary circuit and the release of gas from liquid to gas phase is possible.

At present, NPPs are not working at supercritical pressure. However, because the nominal pressure of the new NPPs is about 160 bars, it is quite possible to postulate transients where the supercritical pressure may be achieved. Thus, the

simulation capabilities at supercritical pressure area may be needed. The APROS six-equation model already currently includes readiness for the simulation of thermal hydraulics at supercritical pressures.

With the developed configuration, the two-fluid model of the APROS code is a well-validated and versatile tool and is ready for many types of nuclear and combustion power plant applications. In particular, it is a practical instrument for the safety analyses of new NPPs and for examinations of plant safety in the case of plant modifications.

In many cases, the one-dimensional two-phase flow simulation provides reliable results. However, in large volumes of the reactor pressure vessel and the core, three-dimensional two-phase flow simulations are often required. Already at this time, advanced computer technology enables the use of three-dimensional two-phase flow models in certain parts of the reactor circuit. Therefore, in the APROS six-equation model as well, the possibility for calculation of three-dimensional two-phase flow should be developed.

References

Barre, F. and Bestion, D. Validation of CATHARE system code for nuclear reactor thermalhydraulics. ASME & JSME Fluid Engineering Conference, August 13–18, 1995, Hilton Head, South Caroline, USA.

Berenson, P.J. Film-Boiling Heat Transfer from a Horizontal Surface. Journal of Heat Transfer, August 1961, pp. 351–358.

Bishop, A. A., Sandberg, R.O. and Tong, L.S. Forced convection heat transfer to water near critical temperatures and supercritical pressures. Report WCAP–5449, Westinghouse Electrical Corporation, Atomic Power Division (1965).

Clement, P. and Regnier, P. Heat Transfer Modelling at the Quench Front during Reflooding Phase of a LOCA (Interpretation of Experimental Results). Meeting of the European Two Phase Flow Group. Stockholm, May 29 – June 1, 1978.

Deruaz, R. and Tellier, N. Comparison Report on OECD-CSNI LOCA Standard Problem n° 7. Idaho 1979. OECD-CSNI, Working Group on Emergency Core Cooling in Water Reactors, CSNI/Report n° 55. 17 p.

Dittus, F.W. and Boelter, L.M. Heat Transfer in Automobile Radiators. Int. Comm. Heat Mass Transfer, Vol. 12, pp. 3–22, 1985, Pergamon Press Ltd.

Edwards, A.R. and O'Brien, T.P. Studies of phenomena connected with the depressurization of water reactors. Journal of the British Nuclear Society 9(1970)2, pp. 125–135.

Freitas, R. and Bestion, D. On the prediction of flooding phenomenon with the CATHARE code. NURETH 6th, October 1993.

Glaeser, P. Downcomer and tie plate countercurrent flow in the Upper Plenum Test Facility. North-Holland, Nuclear Engineering and Design 133 (1992), pp. 335–347.

Glantz, T. and Freitas, R. Improvement of the CAHTHARE 3D Code Prediction on PIERO Transient. 16th International Conference on Nuclear Engineering, May 11–15, 2008, Orlando, Florida, USA.

Groeneveld, D.C. and Snoek, C.W. A Comprehensive Examination of Heat Transfer Correlations Suitable for Reactor Safety Analysis. Multiphase Science and Technology, Volume 2, 1986, pp. 181–274.

Heat Transfer Correlations in Nuclear Reactor Safety Calculations, Vol. II. Publ. Nordic liaison committee for atomic energy. Stockholm 1985. 70 p.

Hänninen, M. A Solution of one-dimensional flow and heat transfer processes with difference method. Thesis for the degree of licentiate of technology, Lappeenranta University of Technology, Department of energy technology (1989).

Hänninen, M. Implementation and validation of downcomer and upper tie plate CCFL-correlations in a two-fluid code. Proceedings of the 16th International Conference on Nuclear Engineering, ICONE16 May 11–15, 2008, Orlando, Florida.

Hänninen, M. and Ahtinen, E. Simulation of non-condensable gas flow in two-fluid model of APROS – Description of the model, validation and application. Annals of Nuclear Energy 36 (2009), pp. 1588–1596.

Hänninen, M. and Kurki, J. Simulation of flows at supercritical pressures with a two-fluid code. NUTHOS-7: The 7th International Topical Meeting on Nuclear Reactor Thermal Hydraulics, Operation and Safety, Seoul, Korea, October 5–9, 2008.

Hänninen, M. and Ylijoki, J. The on-dimensional separate two-phase flow model of APROS. Espoo 2008. VTT Tiedotteita – Research Notes 2443. 61 p. http://www.vtt.fi/inf/pdf/tiedotteet/2008/T2443.pdf

Hänninen, M. and Ylijoki, J. The constitutive equations of APROS six-equation model, Report, VTT Technical Research Centre of Finland, October 2005.

Hölzer, B. Specification of OECD standard problem No. 6, GRS-Garching, Batelle-Frankfurt, 1977.

International Association for Properties of Water and Steam: Revised Release on the IAPWS Industrial Formulation 1997 for the Thermodynamic Properties of Water and Steam, Aug 2007.

Jackson, J.D. and Hall, W.B. Forced convection Heat Transfer to Fluids at Supercritical Pressure. In: Turbulent Forced Convection in Channels and Bundles. 2, edited by S. Kakaç and D. B. Spalding, Hemisphere, 1979.

Jackson, J.D. A Semi-empirical model of turbulent convective heat transfer to fluids at supercritical pressure. Proceedings of the 16th International Conference on Nuclear Engineering, ICONE16 May 11–15, 2008, Orlando, Florida.

Juslin, K. and Silvennoinen, E. Real-Time Solution Approach for Sparse Network Equations. Espoo, Finland, Technical Research Centre Of Finland, Research Notes 615, 38 p. + app. 5 p. ISBN 951-38-2050-5, 1986.

Kurki, J. and Seppälä, M. Thermal Hydraulic Transient Analysis of the High Performance Light Water Reactor Using APROS and SMABRE. 20th International Conference on Structural Mechanics in Reactor Technology (SMiRT 20), Espoo, Finland, August 9–4, 2009, SMiRT 20 – Division X, Paper 3164.

Lilja, R. and Juslin, K. Fast calculation of material properties applied to water and steam. Espoo 1987. Technical Research Centre of Finland, VTT Research Notes 807. 30 p.

Lockhardt, R.W. and Martinelli, R.C. Proposed Correlation of data for isothermal two-phase, two-component flow in pipes. Chemical Engineering Progr. 45 (1), 1949, pp. 39–48.

Miettinen, J. A. Thermohydraulic Model OF SMABRE for Light Water Reactor Simulations. Licentiate Thesis. Helsinki University of Technology, September 1999, Espoo.

Mitchell, R. and Zhao, H. TVO I/II Modernization: Input Data to LOCA Analyses with the GOBLIN/DRAGON Code. ABB Atom Report NTE 96-006 February 1996.

Norrman, S. Modeling of the TVO Nuclear Power Plant with APROS and Calculation of Verification Cases. VTT Research Report ENE4/52/95.

Pioro, I., Duffey, R. and Dumouchel, T. Hydraulic resistance of fluid flowing in channels at supercritical pressures (survey). Nuclear Engineering and Design, 231, 2004, pp. 187–197.

Plit, H.R., Porkholm, K. and Hänninen, M. Validation of the APROS Thermal-hydraulics against the PACTEL test facility. 8th International Topical Meeting on Nuclear Thermal-hydraulics, Kyoto, Japan, September 30 – October 4, 1997.

Plit, H., Kontio, H., Kantee, H. and Tuomisto, H. LBLOCA Analyses with APROS to Improve Safety AND Performance of Loviisa NPP. OECD/CSNI Workshop on Advanced Thermal-Hydraulic and Neutronic Codes: Current and Future Applications, Barcelona, Spain, 10-13 April, 2000.

Properties of Water and Steam in SI-Units. Ed. Schmidt, E. & Grigull, U. 3. ed. Berlin 1982. 194 p.

Purhonen, H., Puustinen, M., Riikonen, V., Kyrki-Rajamäki, R. and Vihavainen, J. PACTEL integral test facility – Description of versatile applications. Annals of Nuclear Energy 33, (2006), pp. 994–1009.

Puska, E.K., Hänninen, M., Porkholm, K. and Kontio, H. Assessment of APROS against the Loviisa-2 Stuck-open Turbine By-pass Valve Transient, ANS, FED-VOL. 204, Power Plant Transients, Book No. G00928–1994.

Puska, E.K. and Porkholm, K. Plant Analyser of Loviisa NPP. Proceedings of the International Topical Meeting on Advances in Mathematics, Computations and Reactor Physics. Pittsburgh, PA, 28 April – 1 May 1991. La Grange Park, IL: American Nuclear Society. Pp. 12.2 4-1–12.2 4-12.

Rajamäki, M. and Narumo, T. Six-equation SVAF model for two-phase with correct propagating velocities of disturbances. Int. J. Numerical Heat Transfer, Part B, 28, 1995, pp. 415–436.

Rajamäki, M. and Saarinen, M. Accurate One-dimensional Computation of Frontal Phenomena by PLIM. Journal of Computational Physics, 1994. Vol.110.

Ransom, V.H., Wagner, R.J, Trap, J.A., Feinauer, L.R., Johnsen, G.W., Kiser, D.M., Riemke, R.A. RELAP5/MOD2 Code Manual Volume 1: Code Structure, Systems, Models, and Solution Methods, NUREG/CR-4312 EGG-2396. 1985.

The RELAP5-3D Code Development Team. RELAP5-3D Code Manual. INEEL-EXT-98-00834, Revision 2.4, June 2005.

Sarrette, C. Effect of Noncondensable Gases on Circulation of Primary Coolant in Nuclear Power Plants in Abnormal Situations. Doctoral Thesis, Lappeenranta University of Technology, Department Of Energy Technology, February 2003.

Siikonen, T. Numerical Method for One-dimensional Two-phase Flow. Numerical Heat Transfer 12(1987), pp. 1–18.

Spore, J.W., Elson, J.S., Jolly-Woodruff, S.J., Knight T.D., Lin, J.-C., Nelson, R.A., Pasamehmetoglu, K.O., Steinke, R.G., Unal, C., Mahaffy, J.H. and Murray, C. TRAC-M/FORTRAN 90 (Version 3.0) Theory Manual. Los Alamos, Los Alamos National Laboratory. LA-UR-00-910. 2000. 923 p.

Stosic, Z.V. and Stevanovic, V.D. Advanced Three-dimensional Two-Fluid Porous Media Method for Transient Two-Phase Flow Thermal-Hydraulics in Complex Geometries. Numerical Heat Transfer, Part B, 41, 2002, pp. 263–289,

Teschendorff, V., Austregesilo, H. and Lerchl, G. Methodology, status and plans for development and assessment of the code ATHLET. Proceedings of the OECD/CSNI Workshop on Transient Thermal Hydraulic and Neutronic Codes Requirements. Annapolis, USA, 1996, pp. 112 – 128.

Wallis, G.B. One-dimensional Two-phase Flow. McGraw-Hill, Inc., New York, 1969.

Wallis, G.B. Phenomena of Liquid Transfer in Two-phase Dispersed Annular Flow. International Journal of Heat and Mass Transfer 11(1968), pp. 783–785.

Vihavainen, J., Hänninen, M. and Tuunanen, J. Improved Thermal Stratification Modeling in the APROS Code Simulations of Passive Safety Injection Experiments. Ninth International Topical Meeting in Nuclear Reactor Thermal Hydraulics (NURETH-9), San Francisco, California, October 3–8, 1999.

Ylijoki, J., Normann, S. and Silde, A. Validation of APROS version 5.08. Research Report, VTT-R-03692-08, 2008.

Ylijoki, J. Kitkan ja faasien välisen lämmönsiirron laskenta kaksifaasivirtatusmallissa. Master's Thesis in Helsinki University of Technology (In Finnish), Espoo, Finland, 1991.

Ylijoki, J. Validation of APROS Model for Olkiluoto Nuclear Power Plant. VTT Research Report PRO5/7830/03. December 2003.

Appendices III and IV of this publication are not included in the PDF version. Please order the printed version to get the complete publication (http://www.vtt.fi/publications/index.jsp).

Publication I

Implementation and validation of downcomer and upper tie plate CCFL correlations in a two-fluid code

In: Proceedings of the 16th International Conference on Nuclear Engineering, ICONE16, May 11–15, 2008, Orlando, Florida, USA.

Proceedings of the 16th International Conference on Nuclear Engineering
ICONE16
May 11-15, 2008, Orlando, Florida, USA

ICONE16-48136

IMPLEMENTATION AND VALIDATION OF DOWNCOMER AND UPPER TIE PLATE CCFL CORRELATIONS IN A TWO-FLUID CODE

Markku Hänninen
VTT Technical Research Centre of Finland
P.O.Box 1000, FI-02044 VTT, Finland

ABSTRACT

At the moment the two-fluid system code APROS has CCFL (Counter Current Flow Limitation) correlations that are designed only for a single pipe or for bundle geometry. In the reactor pressure vessel the downcomer and the upper tie plate of the core are components that call for special CCFL correlations. In the present task the Glaeser CCFL correlations for a downcomer and an upper tie plate have been implemented in the code. The implemented correlations have been validated by calculating several downcomer and upper tie plate test cases of the UPTF (Upper Plenum Test Facility). In the tests the steam flow, the emergency core cooling flows, injection locations and the pressure levels were varied. In the validation the UPTF facility has been modeled with a nodalization, which is normally used in the corresponding calculations. Because the calculation results do not depend merely on the CCFL correlations the new Kutateladze coefficients of the Glaeser correlation had to be specified during the validation. With the selected coefficients, good, slightly conservative results were obtained.

In the paper the work done with the correlations and the results of the validation calculations are described.

1 INTRODUCTION

The six-equation solution system of APROS is in a normal way based on the one-dimensional conservation equations of mass, momentum and energy. When the equations are applied for the liquid and gas phases, all together six partial differential equations are used. In the six-equation model the gas phase may contain also non-condensable gas. The non-condensable gas is assumed to stay in the gas phase, i.e. the dissolution in liquid phase is not taken into account. In addition, it is assumed that non-condensable gas and steam form a homogeneous mixture having the same temperature and the same velocity.

With the assumptions presented above only the mass conservation equation for the non-condensable gas is needed in addition to the normal conservation equations of the six-equation model. Constitutive equations for wall friction, interfacial friction, wall heat transfer and interfacial heat transfer are needed to couple the conservation equations.

At the moment APROS has CCFL (Counter current flow limitation) correlations, which are meant for single pipe or for bundle geometry. In the reactor pressure vessel the downcomer and the upper tie plate of core are components which call for special CCFL correlations. In the present task the Glaeser CCFL correlations for a downcomer and a upper tie plate are implemented in APROS. These correlations are of the Kutateladze-type based on the experiments of the UPTF (Upper Plenum Test Facility). UPTF is a full scale test facility for investigating the counter-current flow through the upper tie plate and through the downcomer in case of emergency cooling as a consequence of large break LOCA/3/. When implementing the CCFL correlation it is changed to the form of the interface friction coefficient. In the model the limiting void fraction has been taken into account.

The implemented correlations have been validated by calculating several downcomer and upper tie plate test cases of the UPTF/6/. In the tests the steam flow, the ECC (Emergency Core Cooling) flows, injection locations and the pressure levels were varied. In the validation the UPTF facility was modelled with a nodalization, which is normally used in the corresponding calculations. Because the calculation results do not depend merely on the CCFL correlations the new Kutateladze coefficients of the Glaeser correlation had to be defined during the validation. With the selected coefficients good slightly conservative results were obtained, i.e. the liquid flows down to the core were in general somewhat less than the in the experiment.

2 DESCRIPTION OF CCFL CORRELATIONS

The CCFL correlations are usually correlated by using the dimensionless Kutateladze numbers, i.e.

$$K_g^{1/2} + M_n K_l^{1/2} = C_n \quad (1)$$

The variables K_g and K_l are dimensionless Kutateladze numbers for gas and liquid.

$$K_g = \frac{\rho_g^{1/2} j_g}{\left[\sigma g\left(\rho_l - \rho_g\right)\right]^{1/4}} \quad (2)$$

$$K_l = \frac{\rho_l^{1/2} j_l}{\left[\sigma g\left(\rho_l - \rho_g\right)\right]^{1/4}} \quad (3)$$

where the j_g and j_l are the superficial gas and liquid flows, ρ_g and ρ_l are gas and liquid densities and σ is the surface tension of water.

Glaeser correlation for Downcomer

The original Glaeser downcomer correlation has the form

$$K_g^{1/2}\left(\frac{\nu_g^{2/3}}{g^{2/3} l}\right)^{1/2} + 0.011 K_L^{1/2} = 0.0245 \quad (4)$$

The coefficients have been obtained by correlating Kutateladze numbers for the whole downcomer area A_{DC}, i.e.

$$K_x = \frac{\dot{m}_x}{\rho_x^{1/2} A_{dc}\left[g\sigma\left(\rho_l - \rho_g\right)\right]^{1/4}} \quad (5)$$

where subscript x is g or l.

The term $\frac{\nu_g^{2/3}}{g^{1/3} l} = \frac{\eta_g^{2/3}}{\rho_g^{1/3} g^{1/3} l}$ takes into account the ratio of the local gas velocity to superficial gas velocity.

The parameter l represents the distance between the emergency injection cold leg and the broken cold leg and it is calculated as

$$l = 0.5\pi d_{outer} \sin^2\left(0.5\theta_{ECC-BCL}\right) \quad (6)$$

The term $\theta_{ECC-BCL}$ means the angle between emergency injection loop and broken cold leg.

If the injection comes from several hot legs the arithmetic average of all distance parameters calculated with Equation (6) is used.

When the Glaeser downcomer correlation is presented in the common form of the Kutateladze type CCFL correlation it is

$$K_g^{1/2} + M_{dc} K_l^{1/2} = C_{dc} \quad (7)$$

Where the Kutateladze coefficients are

$$M_{dc} = 0.011 / \left(\frac{\eta_g^{2/3}}{\rho_g^{2/3} g^{1/3} l}\right)^{1/2} \quad (8)$$

$$C_{dc} = 0.0245 / \left(\frac{\eta_g^{2/3}}{\rho_g^{2/3} g^{1/3} l}\right)^{1/2} \quad (9)$$

The correlation is valid when

$$5400 \le \frac{g^{1/3} l}{\nu_g^{2/3}}$$

Glaeser correlation for Upper tie plate

The Glaeser correlation for the upper tie plate has the form

$$K_g^{1/2}\left(\frac{\nu_g^{2/3}}{g^{1/3} l}\right)^{1/2} + 0.014 K_l^{1/2} = 0.027 \quad (10)$$

The parameter l is calculated as

$$l = d_c \sin\left(0.5\theta_{ECC-BHL}\right). \quad (11)$$

The term $\theta_{ECC-BHL}$ means the angle between the emergency injection hot leg and broken hot leg. If the injection comes from several hot legs the arithmetic average of all angles is used in Equation (11).

The common form of Kutateladze type correlation is

$$K_g^{1/2} + M_{tp} K_l^{1/2} = C_{tp} \quad (12)$$

Where the coefficients are

$$M_{tp} = 0.014 / \left(\frac{\eta_g^{2/3}}{\rho_g^{1/3} g^{1/3} l}\right)^{1/2} \quad (13)$$

$$C_{tp} = 0.027 / \left(\frac{\eta_g^{2/3}}{\rho_g^{1/3} g^{1/3} l} \right)^{1/2} \quad (14)$$

The parameter l is calculated

$$l = d_c \sin(0.5\theta_{ECC-BHL})$$

where $\theta_{ECC-BHL}$ is the angle between the emergency injection loop and the broken hot leg.

The characteristic length d_c (diameter of tie plate) is calculated as

$d_c = (4A_{TP} / \pi)^{1/2}$,
when $y > 0.5(d_{UP} - d_c)$.

The variable y is calculated as

$y = v_{ECC} \left(\frac{2z}{g} \right)^{1/2}$, i.e. y is an estimate for how far the emergency coolant flows in the upper tie plate. The parameter z is the height difference between the bottom of hot leg and upper tie plate.

If $y < 0.5(d_{up} - d_c)$ the characteristic length is calculated

$$d_c = 0.5(4A_{tp} / \pi)^{1/2} + 0.5 d_{up} - y .$$

When the countercurrent flow limitation of the tie plate is calculated the problem is the void fraction in the position of the limiting area. The void fraction above and below the tie plate may be very different and the void fraction of the tie plate is not necessary near to either of them.

In reference /4/ the proper way to calculate the flooding void fraction has been presented.

The formula for the limiting void fraction can be calculated with one of two formulas either using the superficial flow of gas or the superficial flow of liquid

$$\alpha_{\lim} = \frac{R\sqrt{J_g^*}}{(R-1)\sqrt{J_g^*} + 1} \quad (15)$$

$$\alpha_{\lim} = \frac{R\left(1 - \sqrt{J_l^*}\right)}{R\left(1 - \sqrt{J_l^*}\right) + \sqrt{J_l^*}} \quad (16)$$

The dimensionless phase velocities are defined as

$$J_g^* = \frac{J_g}{J_0} \quad (17)$$

$$J_l^* = \frac{J_l}{J_0} \quad (18)$$

The variables R and J_0 are obtained from Kutateladze CCFL –correlation (see Eq 1)

$$J_0 = C_n^2 \left(\frac{g(\rho_l - \rho_g)d}{\rho_g Bo} \right)^{1/2} \quad (19)$$

The variable R is calculated as follows

$$R = M_n^2 \left(\frac{\rho_l}{\rho_g} \right)^{1/2} \quad (20)$$

Finally the void fraction used for the branch limiting the counter current flow is chosen

$$\alpha_{cc} = Min[\alpha_{low}, Max(\alpha_{up}, \alpha_{\lim})] \quad (21)$$

The void fraction α_{low} is the input void fraction for the flow from the lower node of the junction. In APROS α_{low} is calculated from gas and liquid flows.

As indicated in reference /4/ the interfacial friction corresponding to Kutateladze correlation can be calculated in form

$$\tau_{is} = \alpha(1-\alpha) \frac{\left(g(\rho_l - \rho_g)\right)^{1/2}}{C_N^4 D} \left[\sqrt{\rho_g} + M_N^2 (1-\alpha) \sqrt{\rho_l} \right]^2 \quad (22)$$

The formula gives the interfacial friction in a single position corresponding to the values obtained from the Kutateladze type correlation.

In the formula it can be seen that the effect of the coefficient M_n on the interfacial friction coefficient is the larger the more liquid is present. The coefficient C_n, on the other hand, effects on the whole interfacial friction coefficient without dependence on the void fraction.

3 VALIDATION

3.1. Simulation model

In Figure 1 the simulation model of UPTF used for the validation of CCFL correlations in downcomer and upper tie plate is shown. The downcomer has been divided horizontally into eight equal channels. In vertical direction the downcomer has been divided into five nodes. This kind of node division represents the typical system code nodalization of downcomer. In the upper part of the downcomer the flow area reduction due to the hot leg penetrations has been taken into account.

The upper tie plate of core has been simulated with one branch. The upper tie plate was simulated in a simple way in order to avoid the three dimensional effect of water separation in upper plenum. In the model the form loss coefficient 0.5 has been used for the junction describing the flow through the upper tie plate.

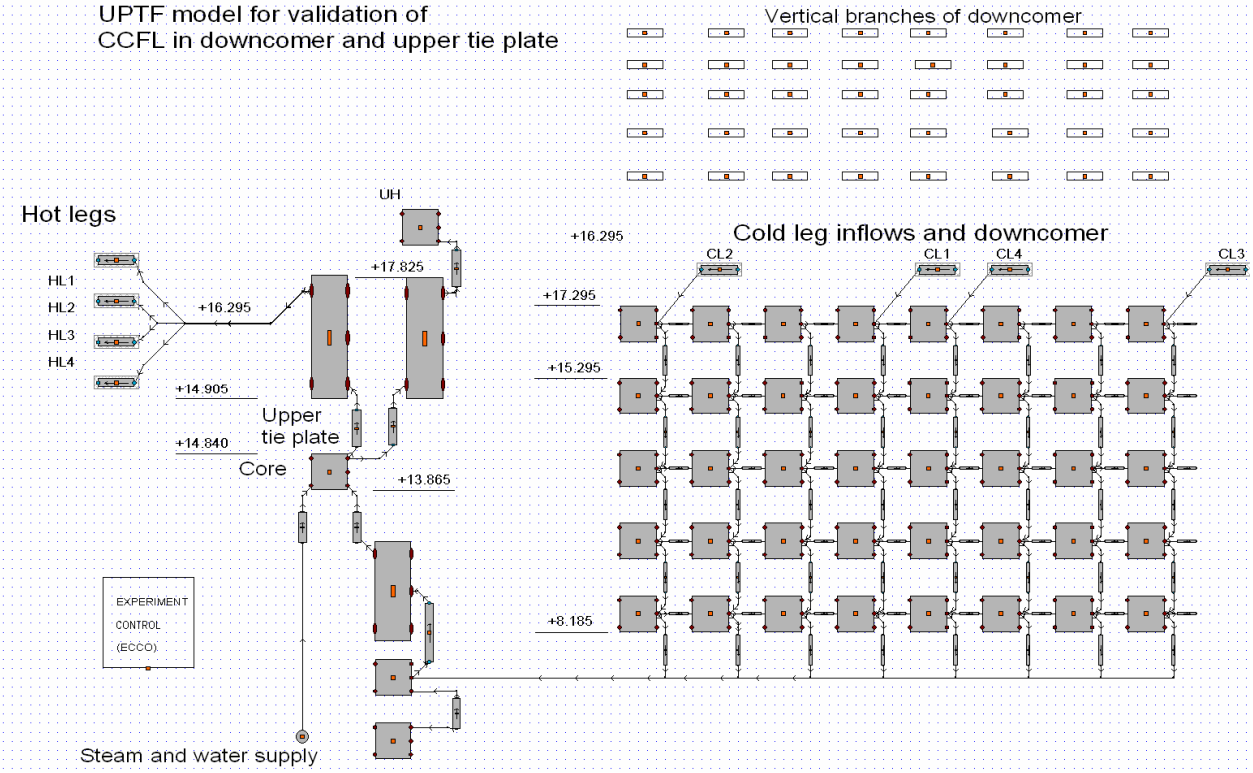

Figure 1. Simulation model of UPTF: used for validation of the CCFL correlation in downcomer and upper tie plate.

3.2. Validation of downcomer CCFL correlation

In validating the CCFL correlations of downcomer seven selected cold leg LOCA experiments of the UPTF facility were calculated. In these experiments the emergency cooling water was injected into downcomer via one or several cold legs. The validation cases were calculated as steady state by keeping the steam flow into the core and the ECC flows into the downcomer as a mass flow boundary. The pressure was tuned by controlling the out flowing leakage mass flow.

During the validation the proper coefficients C_n and M_n for the correlations were defined.

In the calculation the geometric length parameter l value was depended on the ECC injection position. In the experiments 200/I, 200/II and 200/III the injection was from cold leg 1 (near the broken loop) and value of 1.102 was used for geometric length parameter l. In the experiments 201/I and 202/II the value of 6.973 was used for the parameter l (injection from CL2 and CL3). In the experiments 201/III and 203/IV the value of 5.016 was used for parameter l (injection from loops CL1, CL2 and CL3).

The results achieved are shown in Tables 1 and 2. In Figures 2, 3 and 4 the results have been plotted using square roots of the liquid and gas Kutateladze numbers. In general the calculated liquid down flow is close to but less than the experiment values. The measurement uncertainty of down flows is not known accurately. In reference/7/ it is estimated that in loops the uncertainty for liquid density is less that 10 % and for velocity 2 %. These values may be used as estimation to the magnitude of downcomer down flow uncertainty.

In RUN 200/III the relative difference is large (6 kg/s in the experiment versus 57 kg/s as calculated) and the calculated flow is larger than the measured flow. However, if the values of the liquid down flow are compared to the total injection rate 735 kg/s, the relative difference is not very large. It can be stated that when the ECC injection is only into the cold leg near the break, this type correlation applied to the whole downcomer cannot predict properly the down flow.

Table 1. Data of the calculated downcomer experiments (C_n = 0.026215, M_n = 0.0044).

Run No.	Steam into DC (kg/s)	ECC flow into DC (kg/s)	Down flow calculated (kg/s)	Down flow experiment (kg/s)	ECC water sub-cooling ΔT (°C)	Pressure (kPa)
200/I	104	494	**3.0**	**5**	22	451
200/II	54	736	**222**	**351**	9	330
200/III	102	735	**57**	**6**	23	498
201/I	102	CL2: 487 CL3. 490	**845**	**861**	CL2: 10 CL3: 11	330
202/II	128	CL2.486 CL3.491	**512**	**714**	CL2: 13 CL3: 14	416
201III	102	CL1: 493 CL2. 487 CL3. 489	**737**	**942**	CL1:14 CL2:14 CL3:15	414
203IV	51	CL1:493 CL2:485 CL3:487	**1017**	**1031**	CL1:3 CL2:3 CL3:6	337

Table 2. Comparison of calculated and experiment Kutateladze numbers (related for the whole downcomer area 3.6285 m^2).

Run No.	Steam into downcomer (kg/s)	Down flow calculated (kg/s)	Down flow experiment (kg/s)	Calculated $(K_g)^{1/2}$	Experiment $(K_g)^{1/2}$	Calculated $(K_l)^{1/2}$	Experiment $(K_l)^{1/2}$
200/I	104	**3.0**	**5**	2.0	2.0	0.0775	0.100
200/II	54	**222**	**351**	1.54	1.54	0.657	0.826
200/III	102	**57**	**6**	1.94	1.94	0.340	0.110
201I	102	**670**	**861**	2.12	2.12	1.141	1.293
202/II	128	**512**	**714**	2.26	2.26	1.004	1.186
201III	102	**737**	**942**	2.02	2.02	1.204	1.362
203IV	51	**1017**	**1031**	1.49	1.49	1.406	1.416

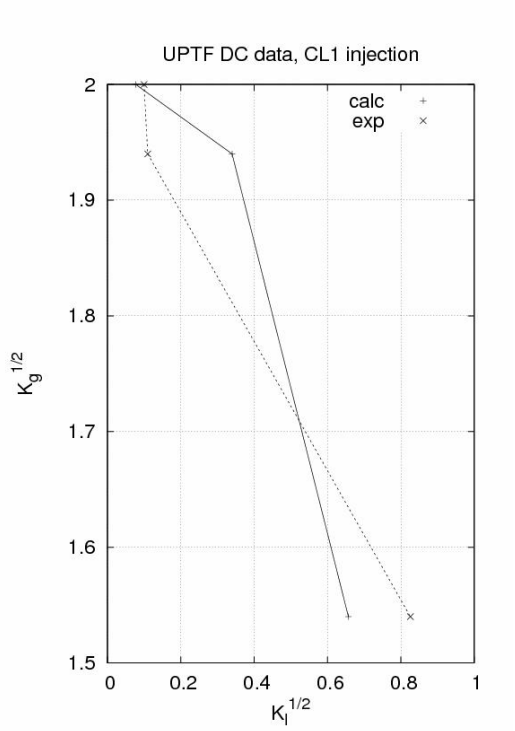

Figure 2. Comparison of calculated and experiment Kutateladze numbers in DC tests with injection from CL1.

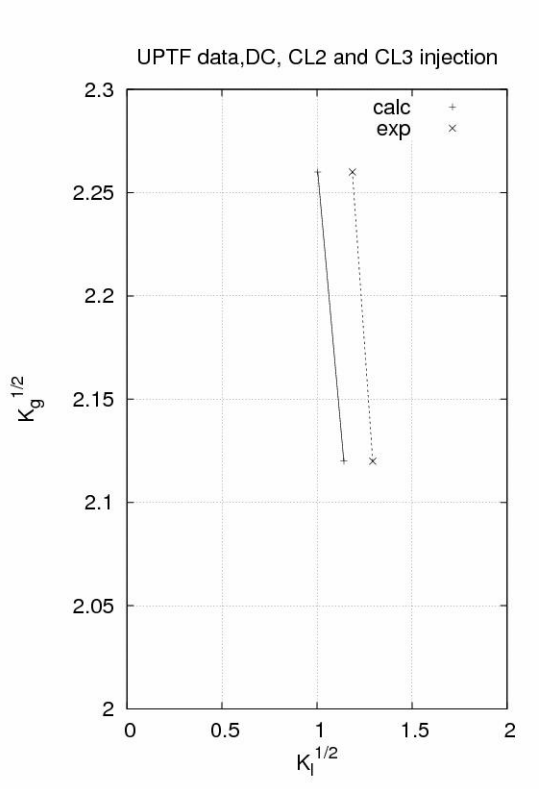

Figure 3. Comparison of calculated and experiment Kutateladze numbers in DC tests with injection from CL2 and CL3.

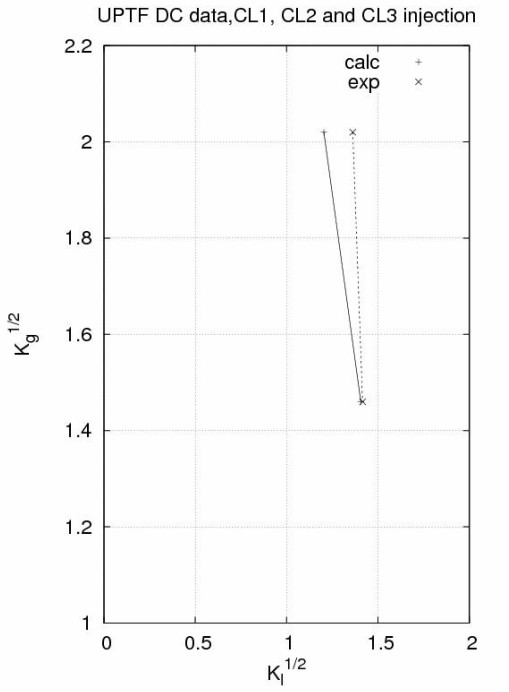

Figure 4. Comparison of calculated and experiment Kutateladze numbers in DC tests with injection from CL1, CL2 and CL3.

3.3. Validation of Upper tie plate CCFL correlation

In the upper tie plate experiments the water level at several positions in the upper plenum was measured. It was found that there was no continuous water level above the upper tie plate. More water was measured in front of the hot legs where water was injected into the upper plenum of the reactor vessel. At other parts of the upper plenum water was carried out to the broken hot leg by the steam flow.

The Glaeser correlation was correlated for the whole upper tie plate and also in the validation the upper tie plate was treated as one junction. During the testing of the model it was found that by using the coefficient 0.027 and 0.014 the calculated down flow was much higher than those in the experiment. According to Glaeser (private communication) there was no pronounced water level above the upper tie plate. More water was measured in front of the hot legs where water was injected via the hot leg ECC nozzles. At the other parts of the upper plenum water was carried out to the broken hot leg by the steam flow.

In the validation, however, the uniform water level above the tie plate was assumed. The same water level of 15 cm was used in each experiment when the liquid down flow was recorded.

Before the final determination of liquid down flow, each validation case had been run into such a steady state that the pressure, ECC injection flows and steam flows had been calmed down. Then the water level was manually reduced slightly below 15 cm and was let to increase again back.

In Tables 3 and 4 the calculated experiments are described and calculated liquid down flows are shown. In the experiments with injection from hot legs HL1 and HL3 (Part 1 experiments) the geometric length parameter used was 1.498. In the experiments with injection from hot leg HL2 (Part 2 experiments) the geometric length parameter of 2.187 was used. The steam flows in the tables are the flows measured in the experiments. The calculated steam Kutateladze numbers are smaller than those from the experiments, because they have been affected by the condensation. The measurement uncertainty of down flows below the upper plate is not known accurately. In reference/7/ it is estimated that in loops the measurement error for density is less that 10 % and for velocity 2 %. These values may be used as estimation to the magnitude of down flow uncertainty.

In Figures 5 and 6 the results have been plotted using square roots of the liquid and gas Kutateladze numbers. In Figure 7 two experiments were calculated with different water levels.

Table 3. Description of the calculated upper tie plate experiments (C_n = 0.005, M_n = 0.00695).

Run No.	Steam flow through upper tie plate (kg/s)	ECC flow into upper plenum (kg/s)	Down flow calculated (kg/s)	Down flow experiment (kg/s)	ΔT (°C)	P (kPa) calc/exp	Water level above tie plate
Part1: 1	172.98	2 x 100	**65**	**76**	29	603/600	0.150
Part 1:2	151.48	2 x 100	**83**	**87**	28	585/588	0.150
Part 1:3	127.46	2 x 100	**100**	**135**	24	542/539	0.150
Part 1:4	103.15	2 x 100	**124**	**142.8**	21	496/496	0.150
Part 1:5	76.54	2 x 100	**167**	**182**	19	464/463	0.150
Part 2:1	215.0	400	**96**	**109**	30	624/620	0.150
Part 2:2	198.33	400	**153**	**243**	35	704/704	0.150
Part 2:3	163.54	400	**202**	**243**	33	674/673	0.150
Part 2:4	130.83	400	**235**	**354**	32	650/652	0.150
Part 2:5	98.48	400	**336**	**324**	26	586/588	0.150
Part 2:6	68.25	400	**402**	**390**	24	520/527	0.050*

Table 4. Comparison of calculated and measured Kutateladze numbers (related for the whole upper tie plate area 3.755 m^2).

Run No.	Steam flow through upper tie plate (kg/s)	ECC flow into upper plenum (kg/s)	$\sqrt{K_g}$ calculated	$\sqrt{K_l}$ calculated	$\sqrt{K_g}$ experiment	$\sqrt{K_l}$ experiment
Part1:1	172.98	2 x 100	2.41	0.358	2.39	0.380
Part 1:2	151.48	2 x 100	2.26	0.405	2,25	0.410
Part 1:3	127.46	2 x 100	2.11	0.443	2.10	0.510
Part 1: 4	103.15	2 x 100	1.92	0.492	1.92	0.530
Part 1:5	76.54	2 x 100	1.66	0.570	1.68	0.590
Part 2:1	215.0	1 x 400	2.66	0.437	2.65	0.460
Part 2:2	198.33	1 x 400	2.45	0.553	2.48	0.690
Part 2:3	163.54	1 x 400	2.26	0.636	2.27	0.660
Part 2:4	130.83	1 x 400	2.01	0.683	2.05	0.710
Part 2:5	98.48	1 x 400	1.72	0.813	1.81	0.800
Part 2:6	68.25	1 x 400	1.40	0.886	1.54	0.870

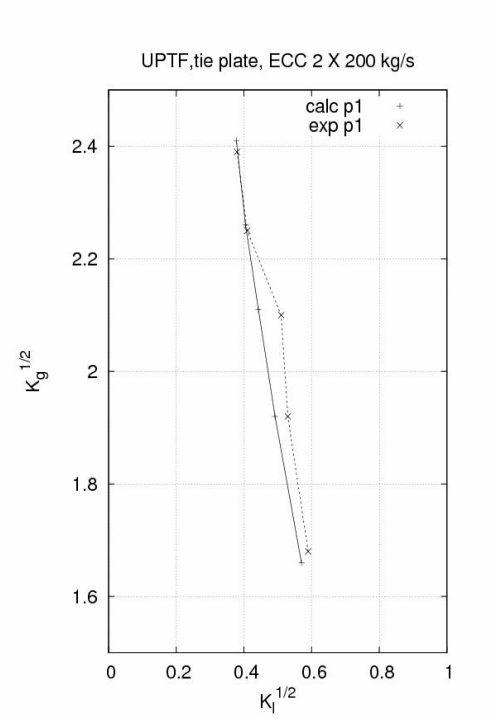

Figure 5. Comparison of calculated and experiment Kutateladze numbers in upper tie plate tests with injection from HL1 and HL3.

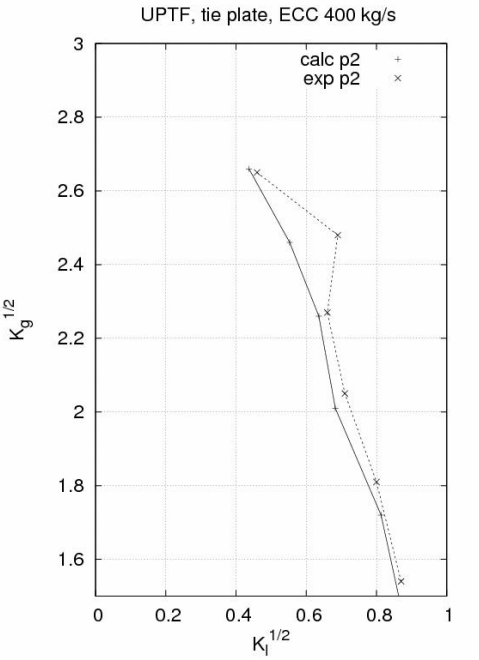

Figure 6. Comparison of calculated and experiment Kutateladze numbers in upper tie plate tests with injection from HL2.

In Figure 7 the effect of the water level is examined by calculating two experiments with different water levels. As it can be seen from the figure the liquid down flow achieves its steady values when the liquid level reaches about 0.07 m. This linear increase of the liquid down is caused by the void fraction change from 1 to 0 above the upper tie. The value of stabilizing point depends on the dimensions and space discretization. Thereafter the mass flow increases only slightly with increasing water level, i.e. the uncertainty of water level above the upper tie plate has not significant effect on the calculation results.

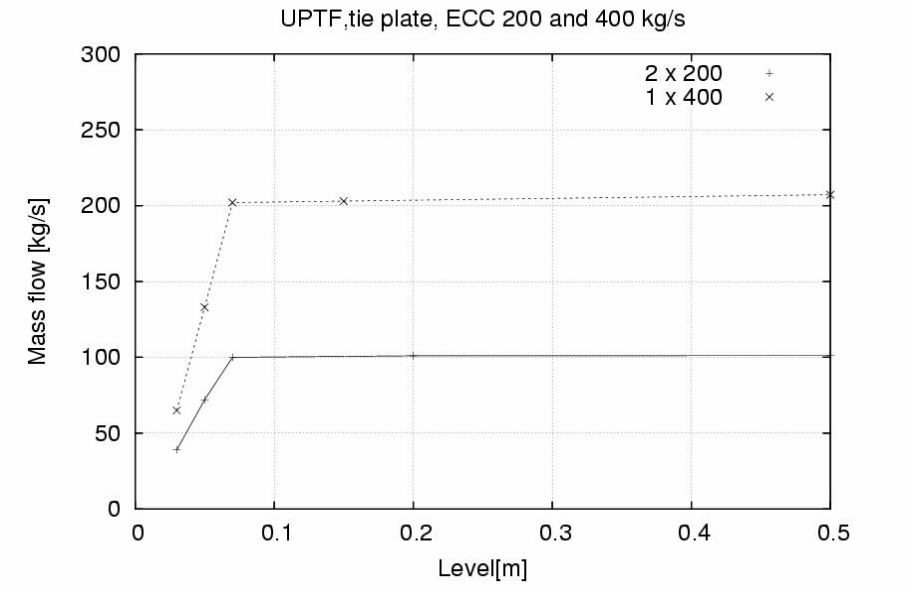

Figure 7. Effect of water level on the down flows: experiments Part1: 3 and Part2:3.

4 CONCLUSION

The new CCFL correlations for the downcomer and the upper tie plate have been implemented in APROS. The correlations are based on the correlations presented by Glaeser /2/. These correlations take into account the distance between the ECC injection cold leg and the broken cold leg in case of the downcomer, and the distance of the ECC injection hot leg and the broken hot leg in case of the upper tie plate. The correlations were validated by simulating several downcomer and upper tie plate tests that had been carried out in UPTF test facility. The test facility was constructed to simulate the ECC cooling in the reactor scale downcomer and upper tie plate. In the tests the steam flow, ECC flows and injection locations and the pressure level were varied. With the aid of calculations the proper coefficients M_n and C_n for the Kutateladze type correlations were defined. The coefficients differed from those given by Glaeser. In case of the upper tie plate the difference between the validated coefficients and those of Glaeser was large. It is expected that the Glaeser correlation represents more phenomena above the upper tie plate. In the validation the correlation was focused on the junction representing solely the upper tie plate. The validation results show that the correlation gives good results in all cases and the predicted liquid down flows are conservative.

NOMENCLATURE

α	Steam volume fraction
Bo	Bond number
C	Coefficient
C_n, M_n	Coefficients in Kutateladze correlation
d	Diameter
d_h	Hydraulic diameter
θ	Angle
g	Acceleration of gravitation
CLn	Cold leg loop n
HLn	Hot leg loop n
J_l, J_g	Liquid and gas superficial velocities
J_0	Parameter used in calculation of dimensionless phase velocities
K_g	Gas Kutateladze number
K_l	Liquid Kutateladze number
l	Geometric distance
$\dot{m}$	Mass flow
p	Pressure
R	Dimensionless variable
ρ_l, ρ_g	Liquid and gas densities
$\overline{\rho}$	Average density
η	Dynamic viscosity
ν	Kinematic viscosity
σ	Surface tension
τ_i	Interfacial friction
u	Velocity

Subscript

BCL	Broken cold leg
BHL	Broken hot leg
c	characteristic
cc	countercurrent
dc	downcomer
ECC	emergency core cooling
f	friction
g	gas
I	interface
l	liquid
lim	limited
low	lower
tp	tie plate
up	upper

ACKNOWLEDGEMENTS

This work was carried out from the initiative of Fortum Nuclear Services Ltd.

REFERENCES

/1/ Hänninen, M., Ylijoki, J., The one-dimensional two-fluid model of APROS, Technical Research Centre of Finland, Technical report HOHTI-2/1992.

/2/ Glaeser, P., Downcomer and tie plate countercurrent flow in the Upper Plenum Test Facility, Nuclear Engineering and Design 133 (1992) 335–347, North-Holland.

/3/ Weiss, P., Emmerling, R., Hertlein, R., Liebert, J., UPTF experiment refined PWR LOCA thermal-hydraulic scenarios: Conclusion from a full-scale experimental program, Nuclear Engineering and Design 149 (1994) 335–347, North-Holland.

/4/ Freitas, R., Bestion, D. “On the prediction of flooding phenomenon with the CATHARE code”, NURETH 6th, October 1993.

/5/ Bestion, D., The physical closure laws in the CATHARE code, Nuclear Engineering and Design 124 (1990) 229–245, North-Holland.

/6/ R. Emmerling et al., UPTF: Program and System Description, U9 414/88/023, November 1988.

/7/ Sarkar, J. Liebert, J., Läufer, R., UPTF Test Instrumentation , Measurement System Identification, Engineering Units and Computed Parameters, 1992.

Publication II

Simulation of non-condensable gas flow in two-fluid model of APROS – Description of the model, validation and application

In: Annals of Nuclear Energy 2009.
Vol. 36, pp. 1588–1596.

Annals of Nuclear Energy 36 (2009) 1588–1596

Contents lists available at ScienceDirect

Annals of Nuclear Energy

journal homepage: www.elsevier.com/locate/anucene

Simulation of non-condensable gas flow in two-fluid model of APROS – Description of the model, validation and application

Markku Hänninen [a,*], Esa Ahtinen [b]

[a] Technical Research Centre of Finland, Nuclear Power Plant Modeling, P.O. Box 1000, 02044 VTT, Espoo, Finland
[b] Fortum Nuclear Services Ltd., P.O. Box 580, 00048 Fortum, Espoo, Finland

ARTICLE INFO

Article history:
Received 8 March 2009
Received in revised form 14 July 2009
Accepted 14 July 2009
Available online 6 September 2009

ABSTRACT

In Loviisa VVER-440 type nuclear power plant the nitrogen used to pressurize hydro-accumulators and other passive safety systems is gradually dissolved to the accumulator water during the long period of normal plant operation. If a primary circuit leakage takes place, the accumulator water is injected into the primary circuit, where lower pressure is prevailing and as a consequence the dissolved nitrogen is released from the liquid phase to gas phase. It is also possible that after the liquid has run out of the accumulator the gaseous nitrogen may flow into the primary system and may thus disturb the circulation in the primary circuit. It is important that the system codes that are used in safety analysis work are capable to simulate flows of non-condensable gases and that they can take into account the release of the dissolved gases. In this paper the non-condensable gas model of the APROS two-fluid safety analysis system code is described. The model has been validated using one experiment carried out in the PACTEL VVER-440 test facility, where the release of the nitrogen dissolved in the accumulator water has been studied. The model has been used to analyze the primary–secondary leakage (PRISE) in the Loviisa nuclear power plant. In this leakage incident the dissolved nitrogen from the accumulator was assumed to flow into the primary circuit of the plant.

1. Introduction

In light water reactors (LWR) the non-condensable gases may affect the behavior of the transients, especially in primary circuit leakages of different break sizes. Thus, the treatment of non-condensable gases has to be taken into account in system codes that are used to analyze the core cooling.

During the long period of normal operation the nitrogen that is used to pressurize hydro-accumulators and other passive safety systems is dissolved into the liquid phase. In case of primary breaks the accumulator water is injected into the primary circuit, where lower pressure is prevailing, and as a consequence the dissolved nitrogen is released from liquid to gas phase.

The two-fluid model of APROS includes separate mass, energy and momentum equations for both liquid and gas phases. The material properties of steam and water are calculated separately for steam and liquid as a function of pressure and as a function of phase enthalpies. By assuming that non-condensable gas forms a homogeneous mixture with steam so that steam and non-condensable gas have the same temperature, and that they flow with the same velocity, only a partial differential equation for the non-condensable gas density is needed for the simulation of the non-condensable gas. In the present thermal–hydraulic model of APROS the non-condensable gas can also be in the form of a dissolved component in the liquid phase. The release of the non-condensable gas from the liquid to gas is calculated if the concentration of the dissolved non-condensable gas is larger than the maximum (saturation) concentration at certain pressure and liquid temperature.

The model has been tested by calculating an experiment carried out in the PACTEL test facility, where the vessel at high pressure included water and steam as well as nitrogen in gaseous form and as dissolved in liquid. In the experiment the gas was let to flow through the orifice, and as a consequence pressure in the vessel decreased. Due to pressure decrease the dissolved gas was released from liquid phase to gas phase, and consequently this caused the water level rise in the tank.

2. Non-condensable gas model

The non-condensable gas model and its relation to the APROS six-equation model is presented in the following. The six-equation model is based on partial differential equations of mass, momentum and energy for liquid and gas phases. By discretizing and linearizing the differential equations four linear equation groups are obtained. With the aid of these discretized equations the pressures, void fractions, phase enthalpies and phase velocities in the simulated system can be solved. The detailed description of the

* Corresponding author. Tel.: +358 40 593 8641; fax: +358 20 722 5000.
E-mail address: markku.hanninen@vtt.fi (M. Hänninen).

0306-4549/$ - see front matter © 2009 Elsevier Ltd. All rights reserved.
doi:10.1016/j.anucene.2009.07.018

Nomenclature

A	flow area (m^2)
a	matrix coefficient
c	heat capacity (J/kg°C)
D	hydraulic diameter of the flow channel (m)
G	mass flux (kg/m^2 s)
g	acceleration of gravity (m/s^2)
h	specific enthalpy (J/kg)
$K(T)$	polynomial used to calculate maximum dissolved gas mole fraction (Pa)
$\dot{m}$	specific mass flow rate (kg/m^3 s)
M	molecular weight of the gas (kg)
p	pressure (Pa)
R	universal gas constant
S	source term
T	temperature (°C)
t	time (s)
u	velocity (m/s)
V	volume (m^3)
x	mass fraction
X	mole fraction
z	space coordinate (m)
Δz	length of junction (m)
α	volume fraction of a phase
η	expansion efficiency
Γ	mass phase change rate (kg/m^3 s)
γ	$\gamma = \frac{c_p}{c_v}$ isentropic exponent
ψ	discharge function
Δh	enthalpy change (J/kg)
Δp	pressure loss or pressure change (Pa)
Δt	time step (s)

Subscripts

d	dissolved, dissolving
g	gas phase, gas mixture
h	constant enthalpy
i	node i, interface
$i-1/2$	junction between nodes $i-1$ and i
$i+1/2$	junction between nodes i and $i+1$
k	gas or liquid phase
l	liquid phase
max	maximum value
nc	non-condensable gas
p	constant pressure
r	release
s	steam
sat	saturation
stat	static
v	constant volume

Superscripts

n	new iteration step
$t-\Delta t$	old time step

Special notations

$[u,0]$	greater of u and 0

two-fluid model of APROS system code has been presented in Hänninen and Ylijoki (2008). In addition to six basic equations the modeling of the non-condensable gas includes the mass equation of the non-condensable gas and the equation for the dissolved gas concentrations. With the aid of these equations the non-condensable gas densities and the dissolved gas concentrations can be solved.

In the model the simulated non-condensable gases are air, nitrogen, helium and hydrogen. For each gas the necessary material properties are calculated. The code has the limitation that only one gas at a time can be simulated.

In the model it is assumed that in gas phase the non-condensable gas and the steam form the homogeneous mixture, i.e. they have the same temperature and velocity. In the dissolved gas model the maximum concentration of the dissolved gas as a function of pressure and liquid temperature is calculated. On the basis of the maximum and the real concentration obtained solving the dissolved concentrations, the released gas flow can be calculated. This released gas is then taken into account in solving the gas phase quantities and the dissolved gas concentrations. On the other hand, if the maximum concentration is larger than the solved concentration, and simultaneously the gas phase includes a large amount of non-condensable gas, the gas is gradually dissolved and the non-condensable gas flow from gas phase to liquid phase is calculated.

In addition to the non-condensable gas densities, the gas temperature has to be calculated iteratively using the calculated gas mixture enthalpy and the densities of steam and non-condensable gas in the gas mixture.

2.1. Solving non-condensable gas in gas phase

For calculating the non-condensable gas densities and pressures in the simulated system the mass transport equation for the non-condensable gas density in gas phase is needed. It can be presented as:

$$\frac{\partial(\alpha_g \rho_{nc})}{\partial t} + \frac{\partial(\alpha_g \rho_{nc} u_g)}{\partial z} = \dot{m}_r \tag{1}$$

In Eq. (1) the subscript g refers to the gas mixture and nc refers to non-condensable gas. The variable $\dot{m}_r$ is the released specific mass flow of the dissolved gas (positive for release, negative for dissolving). For solving numerically the partial differential equations they have to be discretized in respect of time and space. In space discretization the staggered grid is used, i.e. the momentum control volume is different from those of mass and energy. For the space discretization the Eq. (1) is multiplied with flow area A and is integrated over the mesh length Δz, i.e. the mesh volume $V_i = A\Delta z$.

For the time discretization the time derivative is taken in form

$$V_i \frac{(\alpha_g \rho^n_{nc})_i - (\alpha_g \rho_{nc})^{t-\Delta t}_i}{\Delta t} \tag{2}$$

In Eq. (2) the subscript i refers to the mass control volume (node), nc refers to non-condensable gas and g refers to gas mixture. The superscript n is for a new iteration step and $t-\Delta t$ means the previous time step.

Then applying the upwind approach to the convective term in the partial differential Eq. (1), Eq. (3) presented here in discretized form is obtained

$$\begin{aligned} &V_i \frac{\alpha_{g,i}}{\Delta t}\rho^n_{nc,i} - V_i \frac{(\alpha_g \rho_{nc})^{t-\Delta t}_i}{\Delta t} + A_{i+1/2}\alpha_{g,i+1/2}[u_{g,i+1/2},0]\rho^n_{nc,i} \\ &- A_{i-1/2}\alpha_{g,i-1/2}[u_{g,i-1/2},0]\rho^n_{nc,i-1} + A_{i-1/2}\alpha_{g,i-1/2}[-u_{g,i-1/2},0]\rho^n_{nc,i} \\ &- A_{i+1/2}\alpha_{g,i+1/2}[-u_{g,i+1/2},0]\rho^n_{nc,i+1} = V_i \dot{m}_r \end{aligned} \tag{3}$$

In Eq. (3) the non-condensable gas densities with superscript n are unknowns. The subscripts $i-1/2$ and $i+1/2$ refer to junctions coming to or leaving the node i. By rearranging terms in Eq. (3) the matrix type Eq. (4) is obtained. After the total pressures, gas mixture void fractions and phase velocities have been solved the non-condensable gas densities can be solved using Eq. (4).

$$a_i\rho^n_{nc,i} = a_{i+1}\rho^n_{nc,i+1} + a_{i-1}\rho^n_{nc,i-1} + b_i \tag{4}$$

In Eq. (4) the following abbreviations have been used

$$a_i = V_i\frac{\alpha_{g,i}}{\Delta t} + A_{i+1/2}\alpha_{g,i+1/2}[u_{g,i+1/2},0] + A_{i-1/2}\alpha_{g,i-1/2}[-u_{g,i-1/2},0] \tag{5}$$

$$a_{i+1} = A_{i+1/2}\alpha_{g,i+1/2}[-u_{g,i+1/2},0] \tag{6}$$

$$a_{i-1} = A_{i-1/2}\alpha_{g,i-1/2}[u_{g,i-1/2},0] \tag{7}$$

$$b_i = V_i\frac{(\alpha_g\rho_{nc})^{t-\Delta t}_i}{\Delta t} + V_i\dot{m}_r \tag{8}$$

In Eqs. (5)–(8) the junction void fractions are calculated as upwind values, i.e. using the values of the donor node.

When the total pressure, steam and non-condensable gas densities have been calculated the non-condensable gas partial pressure can be solved using simple thermodynamic relations.

The total pressure is the sum of partial pressures of steam and non-condensable gas, Eq. (9).

$$p_g = p_s + p_{nc} \tag{9}$$

The mole fraction of non-condensable gas X_{nc} is calculated with Eq. (10).

$$X_{nc} = \frac{\rho_{nc}}{M_{nc}}\Big/\left(\frac{\rho_{nc}}{M_{nc}} + \frac{\rho_s}{M_s}\right) \tag{10}$$

After the total pressure of gas p_g has been calculated, the partial pressures can be calculated utilizing Eq. (9) and the mole fraction of the non-condensable gas.

In the six-equation model of APROS the linearization of the gas density in respect of pressure is one of key linearizations in solving pressures. When the gas consists of steam and non-condensable gas, the gas density derivative in respect of pressure is calculated as follows:

$$\frac{\partial\rho_g}{\partial p_g} = X_{nc}\left(\frac{\partial\rho_{nc}}{\partial p_{nc}}\right)_h + (1-X_{nc})\left(\frac{\partial\rho_s}{\partial p_s}\right)_h \tag{11}$$

The density derivative of non-condensable gas is calculated from the isentropic gas equation, i.e.

$$\frac{\partial\rho_{nc}}{\partial p_{nc}} = \frac{M_{nc}}{\gamma RT} \tag{12}$$

In the basic six-equation model of APROS the phase enthalpies are solved using the enthalpy equations of liquid and gas mixture.

After the gas mixture enthalpies, and steam and non-condensable densities have been solved the following enthalpy balance can be formed (13).

$$\rho_g h_g(T_g) = \rho_s h_s(T_g) + \rho_{nc} h_{nc}(T_g) \tag{13}$$

The Eq. (13) is needed because the gas mixture temperature T_g cannot be calculated explicitly, but it has to be iterated. The steam temperature is given as a function of steam pressure and enthalpy, while the non-condensable gas enthalpy is calculated using the specific heat capacity (a function of temperature) and the gas temperature.

The non-condensable gas model is a part of the six-equation model, which is calculated iteratively. After every iteration step the gas and liquid mass errors are calculated using the discretized gas and liquid mass equations. The user is able to define the allowed relative mass errors for both gas and liquid individually in each node. For nodes clearly larger than average nodes, a tighter mass error criterion should be used. Usually the relative mass errors below 1d-5 to 1d-6 are achieved. If the mass error criterion is not reached, the model reduces the time step to the half of the presently used time step. Then the iteration is again started from the previous (converged) time point. Also the non-condensable gas mass error is calculated. However, because the non-condensable gas is solved using its own mass equation, the mass error of non-condensable gas is much smaller than the gas mixture mass error providing that the iteration of the whole system has been converged. If the desired accuracy is not reached, the reason is usually in very fast pressure and temperature changes, which may cause large oscillating mass transfer rates between phases.

2.2. Simulation of dissolved non-condensable gas

One goal of the new non-condensable gas model is to simulate the spreading of dissolved gas with liquid flow and to calculate the amount of nitrogen that may release from the liquid phase to gas phase as a consequence of the pressure decrease. Also the slow dissolving of the nitrogen to liquid phase is taken into account.

The dissolved gas in liquid phase is treated as a concentration, i.e. as mass fraction of dissolved gas in liquid phase.

The mass transport equation for dissolved gas can be written in the form

$$\frac{\partial[(1-\alpha)\rho_l x_{nc}]}{\partial t} + \frac{\partial[(1-\alpha)\rho_l u_l x_{nc}]}{\partial z} = -\dot{m}_r \tag{14}$$

When Eq. (14) is discretized in respect of time and space coordinate the numerical model is obtained for solving the spreading of the dissolved gas concentrations. The dissolved gas mass fractions are solved using the standard matrix solver in the APROS code.

In the present model the effect of non-condensable gas on the liquid density is omitted, since the density increase due to the dissolved gas is small compared to the liquid density.

For the model initialization the node related parameter, which defines the initial concentration of the dissolved gas in the liquid phase, is used. The parameter may have values from 0 to 1. The value one means that maximum amount of gas is dissolved in the liquid phase. On the basis of the maximum saturation concentration and the real concentration the six-equation model calculates the released gas flow. If the real concentration is larger than the maximum saturation concentration, the released gas mass flow is

$$\dot{m}_r = (x_{d,nc} - x_{\max,nc})(1-\alpha)\rho_l/\tau_r \tag{15}$$

In Eq. (15) $\dot{m}_r$ is the released mass flow in respect of volume unit (positive direction is for release and negative for dissolving), $x_{d,nc}$ is the mass fraction of nitrogen or other dissolved gas, $x_{\max,nc}$ is the maximum (saturated) mass fraction of dissolved gas, α is the volume fraction of gas, ρ_l is the liquid density and τ_r is the time constant for the release of the dissolved gas.

If the maximum concentration is larger than the real concentration and at the same time the gas phase includes a large amount of non-condensable gas, the gas is gradually dissolved and the small gas flow from gas to liquid is calculated as

$$\dot{m}_d = (x_{d,nc} - x_{\max,nc})\alpha(1-\alpha)\rho_{nc}/\tau_d \tag{16}$$

In Eq. (16) $\dot{m}_d$ is the dissolving mass flow rate in respect of volume unit, ρ_{nc} is the non-condensable gas density and τ_d is the time constant for dissolving.

The maximum mass fraction of the non-condensable gas in liquid phase can be calculated as

$$x_{\max} = \frac{X_{\max}M_{nc}}{X_{\max}M_{nc} + (1-X_{\max})M_{H_2O}} \tag{17}$$

The maximum mole fraction (saturated) can be calculated according to Henry's law

$$X_{\max} = \frac{p_{nc}}{K(T_l)} \tag{18}$$

The term $K(T_l)$ can be presented as a polynomial based on the experimental results (Pray et al., 1952). In reference (Sarrette et al., 1999) the polynomial has been presented in form

$$K(T_l) = 0.57541 \times 10^{10} + 0.13803 \times 10^{9} T_l + 0.94804 \times 10^{5} T_l^2 - 0.13955 \times 10^{5} T_l^3 + 0.68700 \times 10^{2} T_l^4 - 0.95821 \times 10^{-1} T_l^5$$

The release or dissolving mass flows of the non-condensable gas is taken into account in solving the void fractions, in the mass balances of gas mixture and non-condensable gas, in energy balance of gas mixture, in solving the concentrations of dissolved gas, in the energy balance of liquid phase and in the calculation of gas mass errors.

The presented calculation model has been qualitatively verified with a model which describes a simple de-aerator. In the de-aerator model liquid containing plenty of dissolved gas is flowing through a valve into a tank. Due to pressure loss across the valve the liquid is partly evaporated in the de-aerator tank. The mixture of steam and released gas is flowing out from the upper part of the tank. The liquid with lower dissolved gas content is flowing out from the bottom of tank.

2.3. Critical mass flow of non-condensable gas

The critical flow in the APROS six-equation model in water is limited to the value calculated with the Moody model. This works well when the upwind node includes liquid or two-phase water. For non-condensable gas the Moody model is not applicable.

When the flow consists of non-condensable gas the critical mass flow for the gas flow can be calculated as (Linnaluoto, 1965)

$$\dot{m}_{cr} = \mu \psi A \sqrt{p_0 \rho_0} \tag{19}$$

The orifice coefficient μ takes into account friction and contraction of the jet. For well rounded nozzle it is near unity, and for sharp holes in plate it can be as small as 0.59–0.62 (Bohl, 1982). In the equation the discharge function Ψ is calculated as a function of the pressure ratio $z = \frac{p_L}{p_0}$, where p_0 is pressure at upwind state and p_L is pressure at position of the minimum flow area, i.e. where the laval pressure may be achieved.

$$\Psi = \sqrt{2\zeta(1 - z^{1/\zeta'})}\, z^{(\zeta'-1)/\zeta'} \tag{20}$$

The quantity ζ is calculated as a function of isentropic exponent γ

$$\zeta = \frac{\gamma}{\gamma - 1} \tag{21}$$

If necessary the friction can be taken into account with the expansion efficiency η_e, which obtains usually values in the range of 0.94–1 for short pipes. The term ζ' in Eq. (20) is then calculated by dividing ζ' with the expansion efficiency. The critical pressure ratios and other quantities of common gases related to the calculation of the gas critical flow have been presented in Table 1 (Linnaluoto, 1965). The values of helium differ from those of air, nitrogen and hydrogen, because helium is a monoatomic gas.

In the APROS code the maximum non-condensable gas flow is calculated using Eq. (19). In practical applications the gas flow includes always some steam. Thus, the effect of steam on the critical mass flow must be taken into account and the critical flows for steam and non-condensable gas are calculated separately. For steam as

$$\dot{m}_{cr,s} = \mu \Psi_s A \sqrt{p_{0,s} \rho_{0,s}} \tag{22}$$

and for non-condensable gas as

Table 1
Critical pressure ratios and other properties related to the critical flow of different gases.

Gas	p_L/p_0	$\zeta \frac{\gamma}{\gamma-1}$	$\gamma \frac{c_p}{c_v}$	$\psi_{\max}$
Steam	0.546	4.30	1.3	0.667
Helium	0.487	2.50	2.5	0.726
Air	0.528	3.50	1.4	0.685
Nitrogen	0.528	3.50	1.4	0.685
Hydrogen	0.528	3.50	1.4	0.685

$$\dot{m}_{cr,nc} = \mu \Psi_{nc} A \sqrt{p_{0,nc} \rho_{0,nc}} \tag{23}$$

The total critical mass flow is then calculated as the sum of the partial gases mass flows.

3. Validation of the model with PACTEL experiment

In the validation of the non-condensable gas model of APROS one experiment of the PACTEL test facility has been used. The test facility has been originally designed to model the VVER-440 type pressurized water reactor currently in use at Loviisa nuclear power plant in Finland. Nowadays PACTEL is used to model other designs, too. The calculated case simulates transient where the dissolved nitrogen is released in an emergency accumulator due to pressure decreases.

3.1. PACTEL test facility

PACTEL is a volume scaled model in proportion 1:305. To ensure that the gravitational forces remain equal to those in the reference plant, the components preserve the elevation equivalence 1:1 to the reference plant. The test facility consists of primary circuit with a pressurizer, secondary side with steam generators and the emergency core cooling system (Purhonen et al., 2006).

The non-condensable gas model of APROS has been validated against RUN1 experiment where the PACTEL pressurizer was used as a vessel with liquid water and nitrogen at high pressure (Sarrette et al., 1999). The pressure and liquid temperature in the PACTEL pressurizer correspond closely to the conditions in the emergency accumulator of the Loviisa nuclear power plant. The pressurizer was connected to the relief tank with 5 m pipe and release valve. In the pipe there was also a plate with a small hole which was used to measure gas mass flow. The orifice was so small that the flow was assumed to be critical during major part of the experiment. The principle of the test arrangement has been shown in Fig. 1 (Ahtinen, 2008).

In the calculation model the PACTEL pressurizer with the height of 8.8 m was divided into seven nodes with equal lengths in vertical direction. The node center levels from the pressurizer bottom were 0.628 m, 1.885 m, 3.14 m, 4.40 m, 5.66 m, 6.91 m and 8.17 m. In the orifice junction the critical flow limitation with the orifice coefficient of 0.62 was applied. The experiment was calculated using different time constant for nitrogen release. The use of different time constant had no observable effect on the pressure and temperature behavior in the pressurizer tank.

The pressures in the pressurizer and in the relief tank as well as the gas temperature in the upper part of pressurizer have been shown in Figs. 2 and 3, respectively. The calculated results correspond well with the measured values. The pressure decrease in measured data before the opening of the valve was expected to be caused by the leakage.

By comparing the released nitrogen mass flow and the gas mass flow through the orifice in Figs. 4 and 5 it can be seen that the released nitrogen mass flow is less than 1% of value of the mass flow

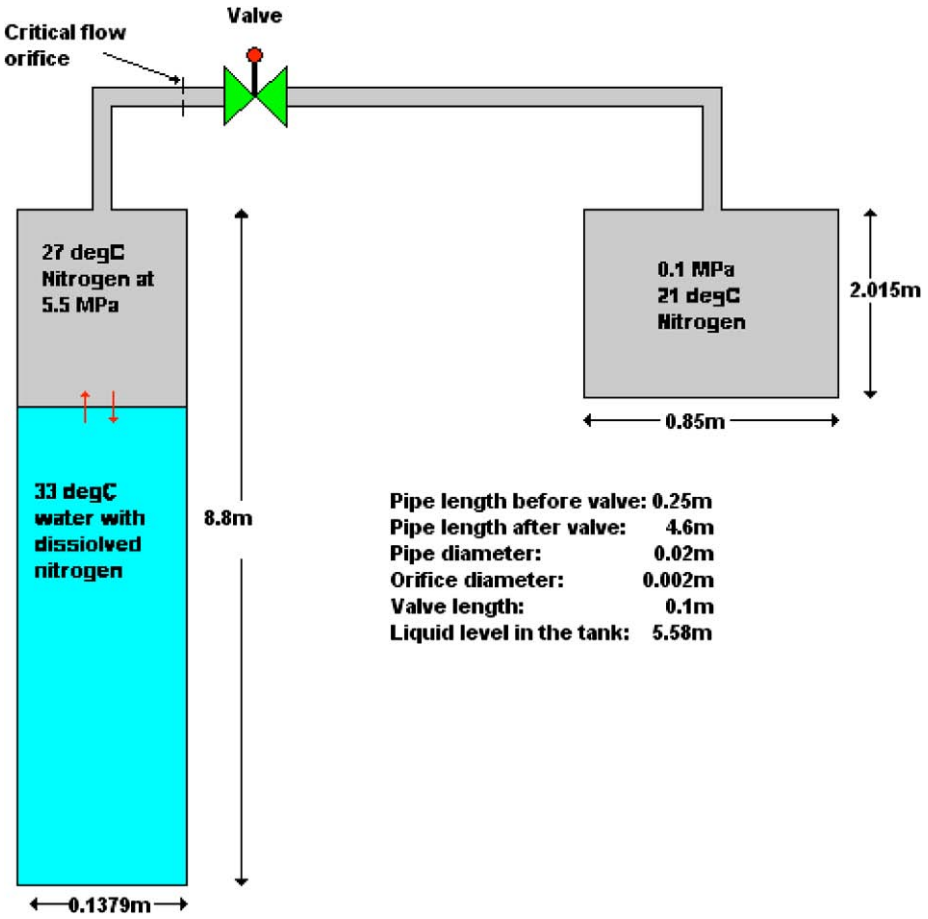

Fig. 1. The arrangement of the test facility.

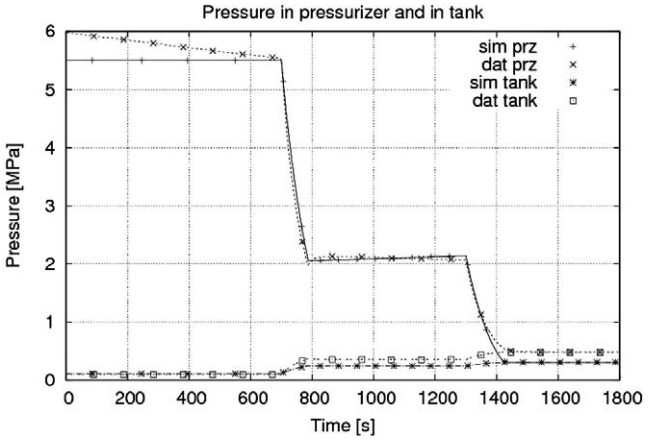

Fig. 2. Simulated and measured pressures in PACTEL pressurizer and relief tank.

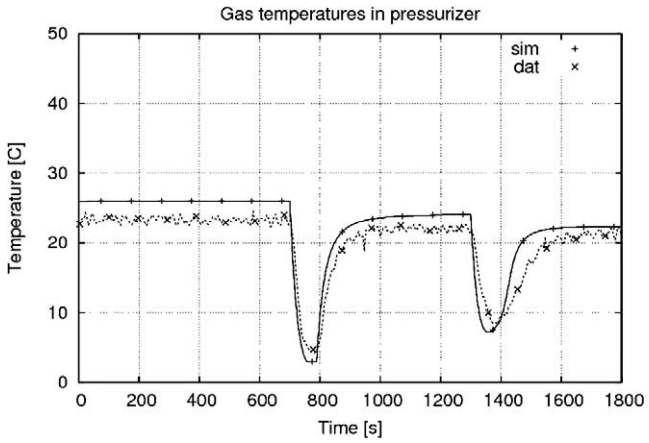

Fig. 3. Calculated and measured gas temperature in upper part of the pressurizer.

through the orifice, and therefore it has practically no effect on the pressure behavior of the pressurizer.

In order find out the effect of the time constant on the release rate of the nitrogen the test RUN1 was calculated using three different time constants 1 s, 50 s and 100 s. The best available measured data which can be used to observe the release rate was the void fraction. Due to pressure decrease the dissolved nitrogen is released and results in increases of gas volume fraction. The volume fraction behavior is also affected by bubble flow upwards in the pressurizer, but it is expected that main effect on void fractions comes from the gas release rates.

In Figs. 6 and 7 the calculated and measured void fractions of the pressurizer on levels 2 m and 3 m in the test facility are shown. It can be seen that during the first nitrogen discharge the measured increase of void fraction is relatively large. None of the calculated cases was able to predict this first fast increase. However, later on, the calculated case with the time constant of 50 s gave the best results in comparison with the measurements. Also in reference (Sarrette et al., 1999) where the release time constant was examined in more detail, the time constant of 50 s was suggested.

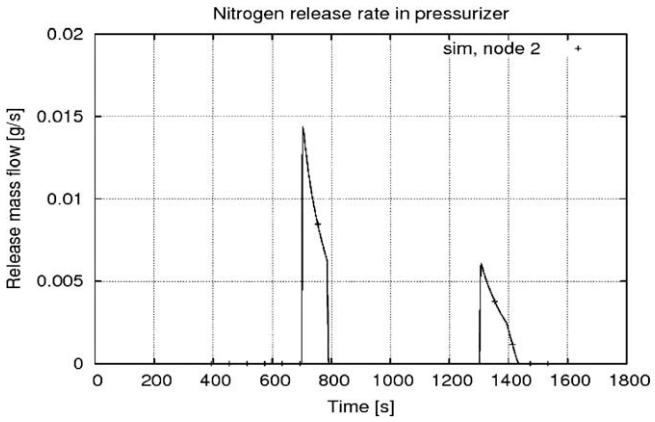

Fig. 4. Released nitrogen mass flow in pressurizer.

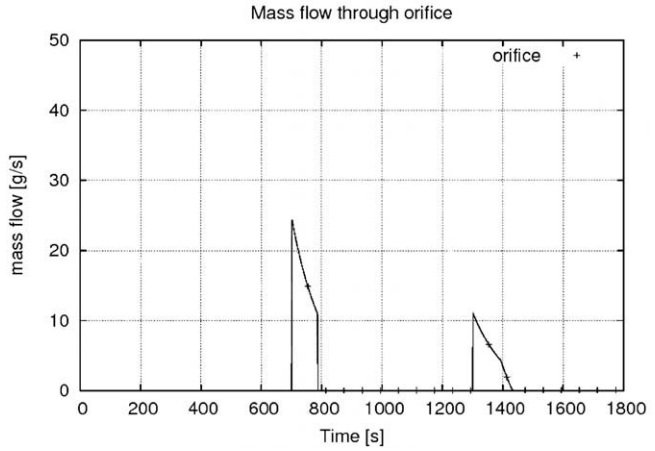

Fig. 5. Discharge gas mass flow through the discharge orifice.

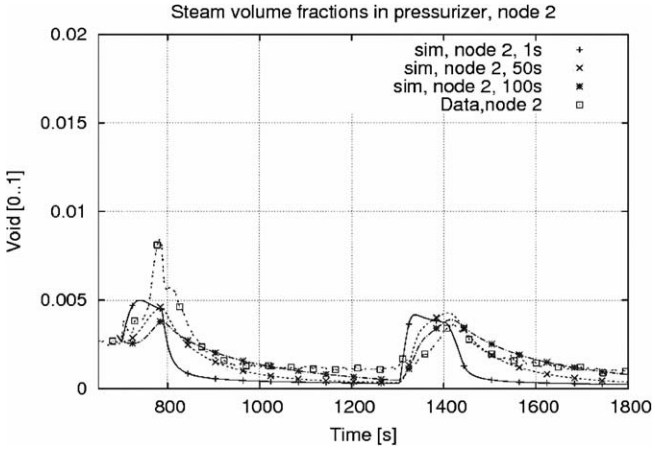

Fig. 6. Calculated and measured gas volume fractions in pressurizer (level of 2 m).

4. Loviisa steam generator collector break simulation

The goal in simulating the steam generator collector break in the Loviisa VVER-440 plant was to examine how the inadvertent injection of one hydro-accumulator, and the possible release of the dissolved nitrogen affect the course of the transient. Loviisa VVER-440 plant has four hydro-accumulators. The total volume of each accumulator is 70 m^3 with 45 m^3 borated water and

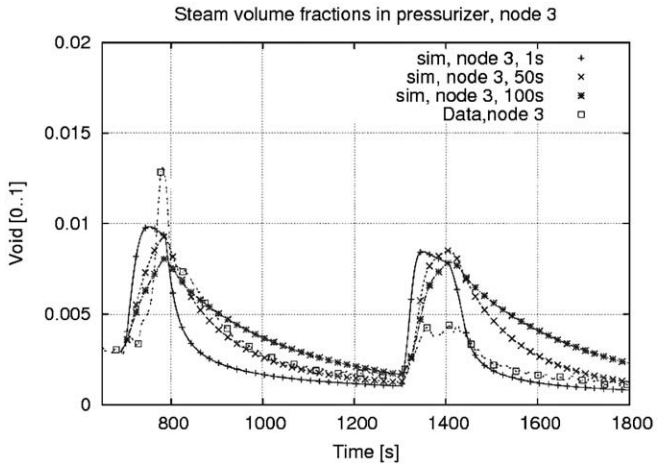

Fig. 7. Calculated and measure gas volume fractions in pressurizer (level of 3 m).

25 m^3 nitrogen gas cushion at 35 bar pressure. Part of the gaseous nitrogen is gradually dissolved to the accumulator water during the long period of normal plant operation. Two of the hydro-accumulators are at 100 °C and other two are at 25 °C temperature. The main task of these passive water tanks is to inject coolant water at rapid rate into the pressure vessel to prevent core uncovering during early phase of a large-break LOCA. During smaller primary circuit leaks, the accumulator injection is not necessarily needed because primary circuit mass balance can be maintained with the help of the high pressure (HP) and low pressure (LP) injection pumps. However, when the pressure is below 35 bar, there is the possibility of an inadvertent injection of one hydro-accumulator. In order to test the new non-condensable gas model of APROS, one of hydro-accumulators is assumed to inject its water into the primary circuit. The injecting accumulator is isolated a few seconds before the water runs out and gas mixture starts to flow into the primary circuit (Ahtinen, 2008).

4.1. Description of the simulated PRISE transient

In the simulated accident the break of 15 cm^2 was assumed in a steam generator cold collector due to the lift up of the steam generator cold collector cover. The primary to secondary type of loss-of-coolant-accidents (PRISE) may result in radioactive coolant flow into the secondary system. If safety valves on the secondary side are stuck open, this radioactive coolant might be released to the environment.

Effective management of the postulated PRISE accident requires certain operative actions. One of the main actions is that in order to terminate the PRISE leak operator has to reduce the primary pressure all the way down to two bar. The depressurization is done by using feed and bleed cooling, i.e. by repetitively varying the pressurizer water level between maximum and minimum allowed limits with the aid of HP or LP injection pumps.

The present simulation begins from the time point, when the primary pressure is below 35 bar and the non-isolated accumulator starts to inject water into the primary circuit. The main parameters describing this depressurization process are shown in the Figs. 8–11. Calculated primary circuit pressure and average temperature are presented in Figs. 8 and 9. Figs. 10 and 11 present the calculated pressurizer water level and PRISE leak mass flow rate. The feed and bleed operations are seen in all calculated values as regular oscillations.

Concerning the new non-condensable gas transport model in APROS code, the main goal was to investigate the behavior of the

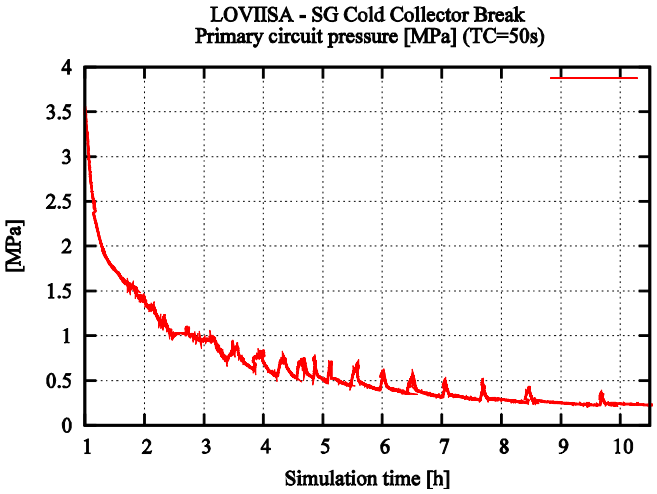

Fig. 8. Primary circuit pressure.

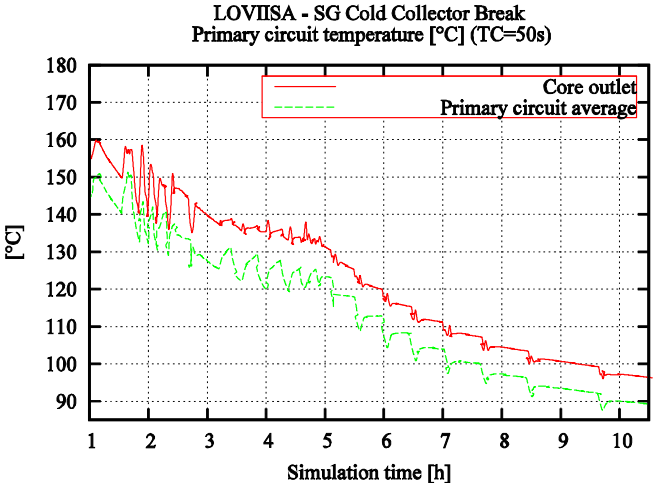

Fig. 9. Primary circuit average and core outlet temperature.

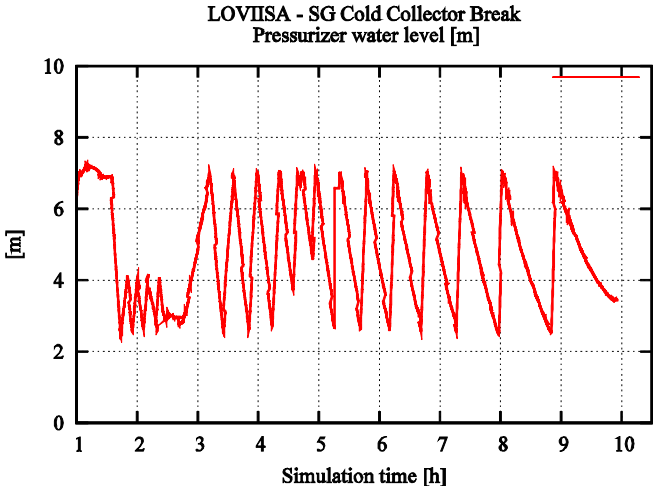

Fig. 10. Pressurizer level.

dissolved nitrogen that is injected from the accumulator into the primary circuit. The main concern is that the primary circuit pressure could decrease so much that the saturation conditions of the dissolved nitrogen are reached in the primary circuit. This would result in release of the dissolved nitrogen from the liquid to gas phase, and as a consequence the prevention of the core cooling.

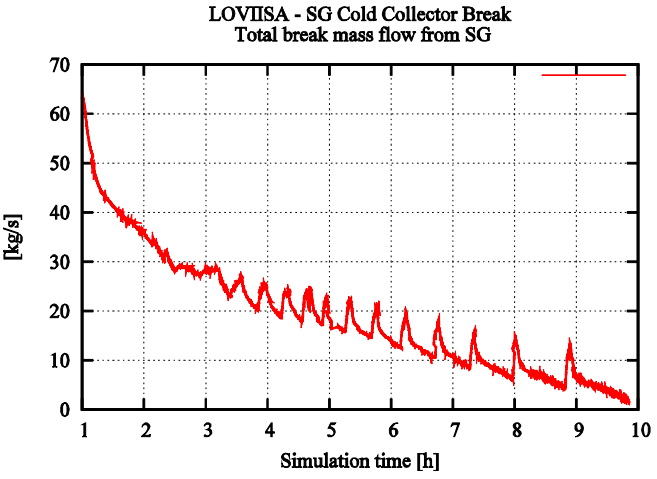

Fig. 11. Break mass flow rate from damaged steam generator.

In order to make appropriate nitrogen mass inventory calculations, following parameters are monitored during the simulation:

- Nitrogen mass in the accumulator gas phase (kg).
- Dissolved nitrogen mass in the accumulator (kg).
- Cumulative nitrogen injection into the primary circuit (kg).
- Cumulative nitrogen leak from damaged SG (kg).
- Total nitrogen mass in the primary circuit (kg).
- Local dissolved nitrogen concentration vs. saturation concentration.

The PRISE simulation was performed using different release time constants. The selected time constants were 10 s, 50 s and 250 s. The dissolution constant was set to 10,000 s in all three cases which practically eliminated dissolution process. As initial condition for the nitrogen inventory calculations the non-isolated accumulator water was assumed to be saturated with dissolved nitrogen. According to Henry's law at 35 bar pressure and 100 °C temperature the dissolved nitrogen mass to be about 21 kg. The mass of the gas phase in the accumulator is about 608 kg. Figs. 12–14 present how the 21 kg of nitrogen gas initially dissolved in accumulator water is divided between the accumulator gas phase and the primary circuit during the injection period. Each fig-

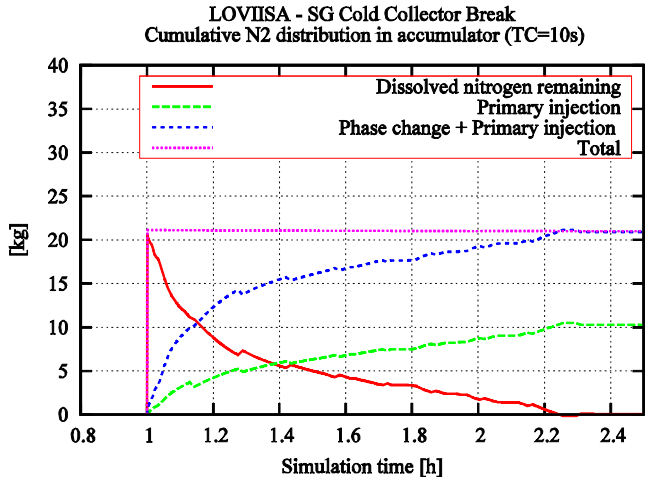

Fig. 12. Distribution of initially dissolved nitrogen with 10 s release time constant.

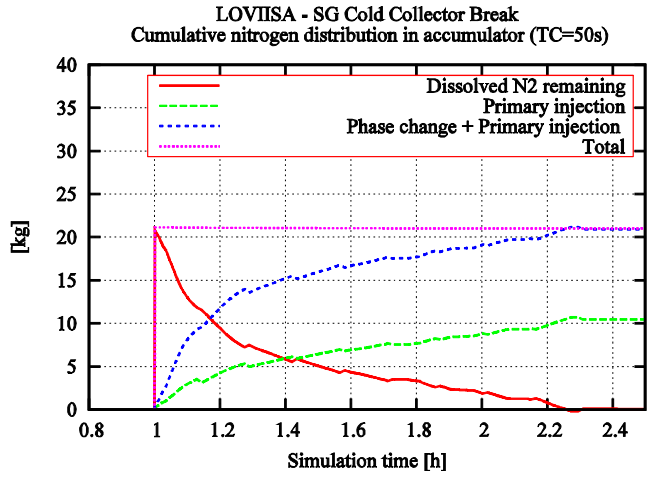

Fig. 13. Distribution of initially dissolved nitrogen with 50 s release time constant.

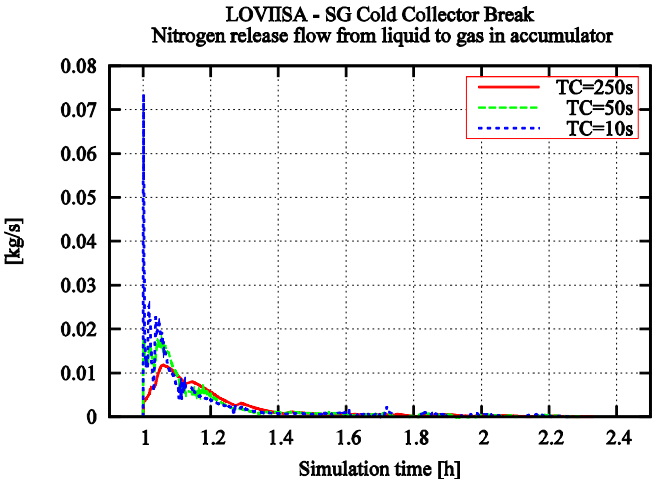

Fig. 15. Nitrogen release mass flow during accumulator injection period.

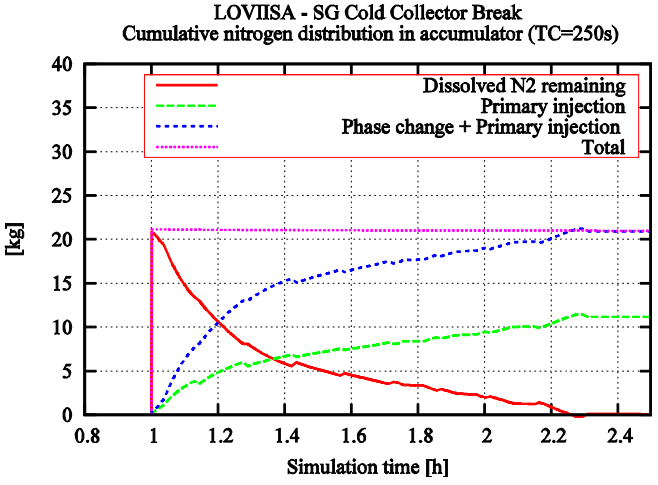

Fig. 14. Distribution of initially dissolved nitrogen with 250 s release time constant.

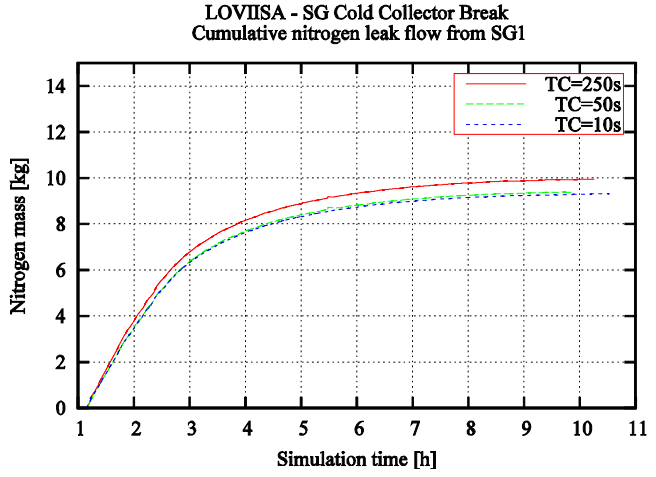

Fig. 16. Cumulative dissolved nitrogen leakage from the damaged steam generator.

ure corresponds to a certain release time constant value. The non-isolated accumulator starts to inject water when the primary pressure is below 35 bar.

It can be observed that the cumulative nitrogen injection into the primary circuit increases from 10 kg to 11 kg when time constant is increased from 10 s to 250 s. Thus, greater amount of the initially dissolved nitrogen is released to the gas phase of the accumulator during the injection period with greater release time constants. The 1 kg difference is rather small and thus the amount of injected nitrogen mass is not very sensitive to size of release time constant. When accumulator water runs out, there is about 618 kg of nitrogen gas remaining in the accumulator. The calculated nitrogen transfer between liquid phase and gas phase is presented in Fig. 15. The time integral of this release flow is the difference between blue and green lines shown in Figs. 12–14.

Fig. 16 presents the cumulative nitrogen mass, which has leaked out from the damaged steam generator during the depressurization period. The cumulative nitrogen leakage is obviously greater with greater release time constant because of the greater cumulative nitrogen injection from the accumulator. One can easily calculate the dissolved nitrogen mass remaining in the primary circuit by subtracting the cumulative nitrogen leakage (Fig. 16) from the cumulative injection presented with green lines in Figs. 12–14.

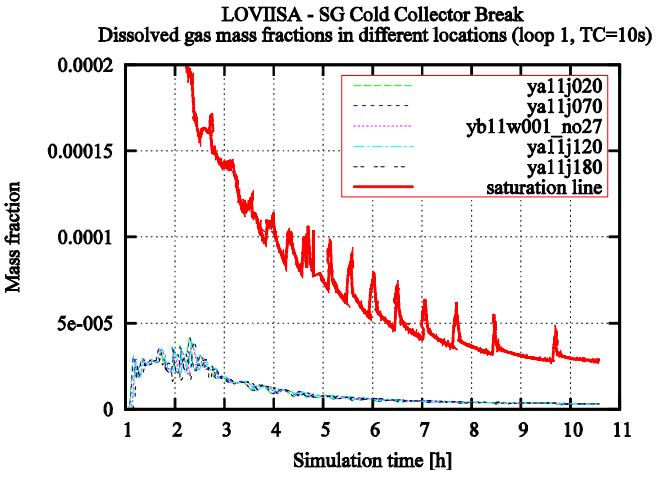

Fig. 17. Local dissolved nitrogen concentrations vs. primary circuit saturation (10 s).

Figs. 17–19 present local dissolved nitrogen concentrations vs. the minimum saturation concentration in the primary circuit with different time constants. As can be noticed, the local dissolved

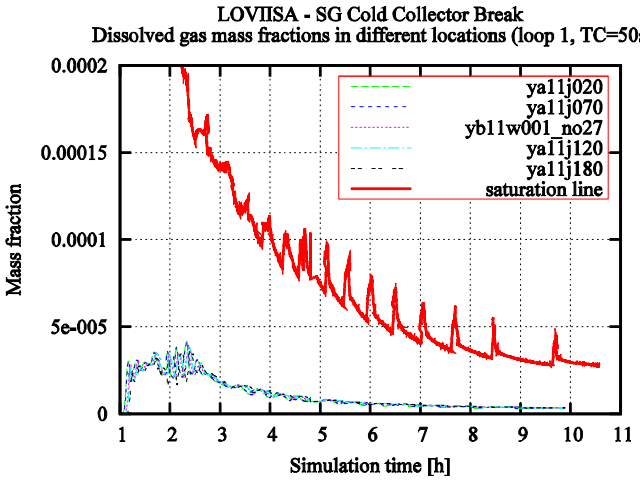

Fig. 18. Local dissolved nitrogen concentrations vs. primary circuit saturation (50 s).

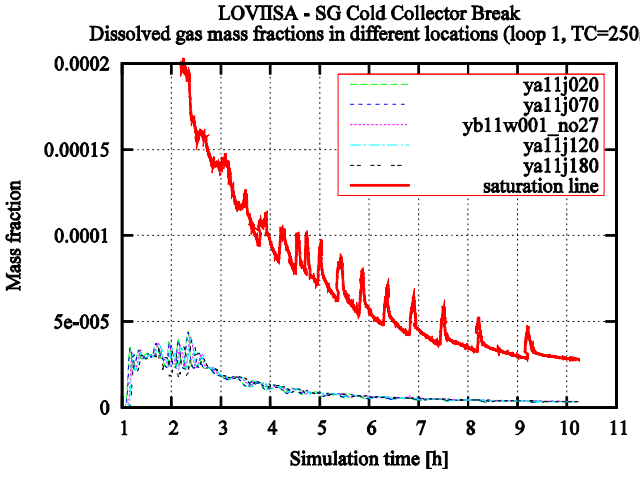

Fig. 19. Local dissolved nitrogen concentrations vs. primary circuit saturation (250 s).

nitrogen concentrations remain well below saturation concentration. Thus, there is no nitrogen gas release during PRISE accident and no potential threat to accident management.

The simulation case presented in this paper was relatively simple since the accumulator was isolated immediately when the water ran out. This assumption caused the cumulative nitrogen injection to be from 10 kg to 11 kg depending on the assumed release time constant. Further simulations where the 618 kg gaseous phase of the accumulator is assumed to be injected into the primary circuit are planned.

5. Conclusions

The two-fluid model of APROS safety analysis code is able to simulate the different non-condensable gas which can be as gaseous form or as dissolved in liquid phase. In the paper the model and its validation have been described in detail. The release time constant which has been used in the model has been estimated with the aid of an experiment made in the PACTEL test facility. The validated model has been applied to calculate a PRISE transient for the Loviisa VVER type nuclear power plant. In the transient one of hydro-accumulators is expected to inject its water including dissolved nitrogen into the primary circuit. The simulations confirmed that the local dissolved nitrogen concentrations remained well below saturation concentration during primary circuit depressurization period. This means that there was no gas release and thus, natural circulation and accident management was not in danger.

Acknowledgments

The authors appreciate to Fortum Nuclear Services Ltd., for funding this work together with VTT Technical Research Center of Finland.

References

Ahtinen, E., 2008. Development and Validation of a New Non-Condensable Gas Transport Model for the APROS Simulation Software. Master's Thesis in Helsinki University of Technology, Espoo, Finland (in English) (Fortum Nuclear Services Ltd.).

Bohl, W., 1982. Teknillinen virtausoppi, Ursprünglich veröffentlicht unter dem Titel "Technische Strömungslehre". Vogel-Verlag, Würzburg. ISBN 951-9405-28-3 (in Finnish).

Hänninen, M., Ylijoki, J., 2008. The one-dimensional separate two-phase flow model of APROS. Espoo. VTT Tiedotteita – Research Notes.

Linnaluoto, V., 1965. Tekniikan käsikirja, Osa 1, Kaasudynamiikka, K.J. Gummerus. pp. 244–254 (in Finnish).

Pray, H.A., Shweickert, C.E., Minnich, B.H., 1952. Solubility of hydrogen, oxygen, nitrogen and helium in water at elevated temperatures. Industrial and Engineering Chemistry 44(5), 1146–1151.

Purhonen, H., Puustinen, M., Riikonen, V., Kyrki-Rajamäki, R., Vihavainen, J., 2006. PACTEL integral test facility – description of versatile applications. Annals of Nuclear Energy 33, 994–1009.

Sarrette, Ch., Kouhia, J., Purhonen, H., Bestion, D., 1999. Noncondensable gas release and dissolution: analytical experiment and calculation with Cathare2 V1.3I. In: Ninth International Topical Meeting on Nuclear Reactor Thermal Hydraulics (NURETH–9), San Francisco California, October 3–8.

Series title, number and report code of publication

VTT Publications 720
VTT-PUBS-720

Author(s)
Markku Hänninen

Title

Phenomenological extensions to APROS six-equation model. Non-condensable gas, supercritical pressure, improved CCFL and reduced numerical diffusion for scalar transport calculation

Abstract

This thesis focuses on the development of the two-fluid model of the APROS simulation program. The system of constitutive equations and how equations are related to basic equations have been presented and discussed. The new non-condensable gas model, which was implemented to the two-fluid model, has been described in detail. The extension of the non-condensable gas model to the two-fluid system and the validation of the model have also been presented. The changes made to the six-equation model when the model has been applied to supercritical pressure calculation have been depicted. Finally, the author describes how the whole complicated s-ystem is verified and validated. Through the simulations, the applicability of the two-phase model for the analyses of real plant applications is substantiated and verified.

In addition to this summary, the thesis consists of four publications. The first paper deals with how the CCFL (Counter Current Flow Limitation) correlations have been implemented to the code and how these correlations have been verified. In the second paper, the non-condensable gas model and its implementation to the two-fluid model have been presented. The third paper describes how the sharp temperature distribution can be maintained in the liquid flow through the aid of simple higher order discretization. In the fourth paper, the modifications carried out to the two-fluid model when applied to the calculation of the supercritical pressure flow are described and discussed.

ISBN
978-951-38-7367-7 (soft back ed.)
978-951-38-7368-4 (URL: http://www.vtt.fi/publications/index.jsp)

Series title and ISSN
VTT Publications
1235-0621 (soft back ed.)
1455-0849 (URL: http://www.vtt.fi/publications/index.jsp)

Project number
32753

Date
November 2009

Language
English, Finnish abstr.

Pages
60 p. + app. 62 p.

Name of project
SAFIR, SAFIR2010

Commissioned by
State Nuclear Waste Management Fund (VYR), VTT, other funders

Keywords
Two-fluid model, two-phase flow, interface heat transfer, interface friction, wall friction, wall heat transfer, boiling crisis, non-condensable gas, dissolved gas, counter current flow limitation, discreatization, validation, supercritical pressure, nuclear power plant, APROS

Publisher
VTT Technical Research Centre of Finland
P.O.Box 1000, FI-02044 VTT, Finland
Phone internat. +358 20 722 4520
Fax +358 20 722 4374

Julkaisun sarja, numero ja raporttikoodi

VTT Publications 720
VTT-PUBS-720

Tekijä(t)
Markku Hänninen

Nimeke

Kuusiyhtälömallin ilmiövalikoiman laajentaminen. Lauhtumattomien kaasujen ja ylikriittisen paineen laskenta, veden ja höyryn vastakkaissuuntaisen virtauksen mallien parantaminen ja numeerisen tasoittumisen vähentäminen

Tiivistelmä

Tämä väitöskirja kuvaa APROS-simulointiohjelmistoon kuuluvan yksidimensioisen veden kaksifaasivirtauksen laskentaan tarkoitetun kuusiyhtälömallin kehityksen. Korrelaatiotyyppiset lisäyhtälöt kuvataan ja samalla kerrotaan, kuinka ne liittyvät perusyhtälöiden muodostamaan ratkaisuun. Perinteisen kaksifaasilaskentamallin lisäksi väitöskirja kuvaa lauhtumattomien kaasujen laskentamallin, sen kelpoistamisen ja kuinka tämä laskentamalli liittyy kaksifaasivirtauksen ratkaisujärjestelmään. Kaksifaasimallia on myös muutettu siten, että sitä voidaan soveltaa ylikriittisen paineen laskentaan. Kaksifaasimalli muodostaa hyvin monimutkaisen järjestelmän, jonka toimivuus pitää varmentaa aina kun jokin uusi osamalli liitetään kokonaisuuteen tai jotakin mallin osaa muutetaan. Väitöskirjassa kuvataan eräiden kaksifaasivirtaukseen ja lämmönsiirtoon liityvien kelpoistamiseen käytettyjen kokeiden laskentaa. Näillä kokeilla osoitetaan kaksifaasimallin toimivuus ja se, että laskentatulokset vastaavat todellisuutta.

Johdannon lisäksi väitöskirja sisältää liitteenä olevat neljä julkaisua. Ensimmäisessä kuvataan faasien vastakkaissuuntaisen virtauksen rajoittamiseen käytettyjen CCFL-korrelaatioiden (Counter Current Flow Limitation) liittäminen laskentajärjestelmään sekä näiden korrelaatioiden kelpoistamiseen liittyvät simuloinnit. Toisessa kerrotaan yksityiskohtaisesti lauhtumattomien kaasujen laskentamallista, sen kelpoistamisesta ja soveltamisesta todelliseen laitostransientin laskentaan. Kolmannessa julkaisussa kuvataan ohjelmaan kehitetty vaihtoehtoinen korkeamman kertaluvun diskretointimenetelmä, jolla pystytään vähentämään numeerista diffuusiota. Neljännessä julkaisussa tarkastellaan ylikriittisen paineen laskennan vaatimia muutoksia kaksifaasimalliin ja kuvataan mallin toimivuutta mittaavien laskentatapauksien simulointeja.

ISBN
978-951-38-7367-7 (soft back ed.)
978-951-38-7368-4 (URL: http://www.vtt.fi/publications/index.jsp)

Avainnimeke ja ISSN
VTT Publications
1235-0621 (nid.)
1455-0849 (URL: http://www.vtt.fi/publications/index.jsp)

Projektinumero
32753

Julkaisuaika
Marraskuu 2009

Kieli
Englanti, suom. tiiv.

Sivuja
60 s. + liitt. 54 s.

Projektin nimi
SAFIR, SAFIR2010

Toimeksiantaja(t)
State Nuclear Waste Management Fund (VYR), VTT, muita rahoittajia

Avainsanat
Two-fluid model, two-phase flow, interface heat transfer, interface friction, wall friction, wall heat transfer, boiling crisis, non-condensable gas, dissolved gas, counter current flow limitation, discreatization, validation, supercritical pressure, nuclear power plant, APROS

Julkaisija
VTT
PL 1000, 02044 VTT
Puh. 020 722 4520
Faksi 020 722 4374

VTT PUBLICATIONS

ISBN 978-951-38-7367-7 (soft back ed.)
ISSN 1235-0621 (soft back ed.)

ISBN 978-951-38-7368-4 (URL: http://www.vtt.fi/publications/index.jsp)
ISSN 1455-0849 (URL: http://www.vtt.fi/publications/index.jsp)